# Spatial implementation of frequency ratio, statistical index and index of entropy models for landslide susceptibility mapping in Al-Balouta river basin, Tartous Governorate, Syria

Hazem Ghassan Abdo[1,2,3*] , Hussein Almohamad[4], Ahmed Abdullah Al Dughairi[4], Sk Ajim Ali[5], Farhana Parvin[5], Ahmed Elbeltagi[6], Romulus Costache[7,8,12], Safwan Mohammed[9,13], Motrih Al-Mutiry[10] and Karam Alsafadi[11]

**Abstract**

Landslide vulnerability prediction maps are among the most important tools for managing natural hazards associated with slope stability in river basins that affect ecosystems, properties, infrastructure and society. Landslide events are among the most hazardous patterns of slope instability in the coastal mountains of Syria. Thus, the main goals of this research are to evaluate the performance of three different statistical outputs: Frequency Ratio (FR), Statistical Index (SI) and Index of Entropy (IoE) and therefore map landslide susceptibility in the coastal region of Syria. To this end, we identified a total of 446 locations of landslide events, based on the preliminary inventory map derived from fieldwork and high-resolution imagery surveys. In this regard, 13 geo-environmental factors that have a high influence on landslides were selected for landslide susceptibility mapping. The results indicated that the FR method outperformed the SI and IoE models with a high AUC of 0.824 and better adaptability, followed by the SI with 0.791. According to the SCAI values, although the FR model achieved the best reliability, the other two models also showed good capability in determining landslide susceptibility. The result of FR-based modelling showed that 18.51 and 19.98% of the study area fall under the high and very high landslide susceptible categories, respectively. In the map generated by the SI method, about 36% of the study area is classified as having high or very high landslide sensitivity. In the IoE method, whereas 14.18 and 25.62% of the study area were classified as "very high susceptible" and "high susceptible," respectively. The relative importance analysis demonstrated that the slope aspects, lithology and proximity to roads effectively motivated the acceleration of slope material instability and were the most influential in both the FR and SI models. On the other hand, the IoE model indicated that the proximity to faults and roads, along with the lithology factor, were important influences in the formation of landslide events. As a result, the statistical bivariate models-based landslide mapping provided a reliable and systematic approach to guide the long-term strategic planning procedures in the study area.

*Correspondence: hazemabdo@tartous-univ.edu.sy

[1] Geography Department, Faculty of Arts and Humanities, University of Tartous, Tartous, Syria
Full list of author information is available at the end of the article

## Introduction

Landslides are classified as one of the most important physical hazards affecting human life, infrastructure and sustainable development (Alsabhan et al. 2022; Nwazelibe et al. 2022). Landslide event occurs when the shear strength of the material, that forms the slope, is greater than gravity and other types of shear stress within a path (Reichenbach et al. 2018a, b; Shi et al. 2020; Karaman et al. 2022). Unlike other natural hazards, the landslide risk assessment process is described as complex due to the difficulty of landslide inventorization and the spatial interaction between the motivating factors (Naceur et al. 2022; Jana et al. 2019; Valiante et al. 2021; Hateffard et al. 2021). Globally, landslides cause a real threat to life by total or partial destruction of infrastructure projects (Emberson et al. 2021; Jamir et al. 2022).

Landslides are among the greatest significant issues that governments strive to reduce their destructive impacts on lives, properties and infrastructure, especially in mountainous areas (Dikshit et al. 2020; Nakileza and Nedala 2020; Batar and Watanabe 2021; Abdo 2022; Rahman et al. 2022). Many studies confirmed that increasing the landslide events are motivated by the spatial integration between physical and anthropological factors (Razavizadeh et al. 2017; Akinci and Yavuz Ozalp 2021; Yamusa et al. 2022; Jaafari et al. 2022). The first fundamental step related to efficient spatial management of landslide risk is the preparation of landslide susceptibility mapping (Das et al. 2022; Guo et al. 2021; Skrzypczak et al. 2021). A landslide susceptibility map, however, delineates zones vulnerable to future landslide events within a given area. the high-quality generation of landslide susceptibility map depends on the effectiveness of the fieldwork, access to the most suitable data, the overall determination of the spatial conditioning factors and the appropriate selection of modelling and simulation methods (Mersha and Meten 2020; Wubalem 2021).

Recently, scientists throughout the world have used many approaches integrated with geographic information systems (GIS) to map landslide susceptibility, including weight of evidence (WoE; Cao et al. 2021); evidential belief functions (EBF; Anis et al. 2019); multivariate logistic regression model (Li et al. 2021a, b; Castro-Miguel et al. 2022), information value (IV) and frequency ratio (FR; Rahman et al. 2022); generalized additive model (Lin et al. 2021); analytical hierarchy process (AHP; Kumar and Anbalagan 2016; Babitha et al. 2022); support vector machine (SVM; Naceur et al. 2022); generalized additive model (GAM; Chen et al. 2017a); digital elevation model

and hazard index (Hamza and Raghuvanshi 2017); multi-criteria decision analysis (MCDA; Pham et al. 2021a).

As such, landslide susceptibility models can be classified into three categories: machine learning-based models, empirical approaches-based models and statistical-driven models. However, each of the aforementioned landslide susceptibility models has its own set of benefits and disadvantages (Reichenbach et al. 2018a, b). The machine learning-based landslide susceptibility models offer superior flexibility and adaptability, but they are limited by the model parameters used and the quantity of the training dataset (Zhou et al. 2018). In spite of the fact that the empirical models make use of past information and experience, the analysis results may differ significantly from the natural conditions (Ghosh et al. 2011). Whilst statistical-based landslide susceptibility models can reflect the relation between input conditional factors and output assessment outcomes, the linear model is very simple and subject to aberrations (Reichenbach et al. 2018a, b). As a result, prior studies demonstrate that the efficacy of established susceptibility models differs depending on various conditioning factors, and no one method is preferable in all settings (Zhou et al. 2018; Argyriou et al. 2022).

According to the current literature, the Mediterranean terrain is one of the areas most affected by the landslides risk (Argyriou et al. 2022; Abdo 2022). The landslide is considered one of the most direct impacts on slope instability in Mediterranean environments (Ullah et al. 2022). Hence, the prediction of landslides is one of the most important pivots of geological and geomorphological studies in these environments, such as Isparta−Antalya highway (D-685), Turkey (Hepdeniz 2020), Ionian Islands, Greece (Mavroulis et al. 2022), Mila town, Algeria (Bounemeur et al. 2022) and the prefecture of Chania, Crete (Psomiadis et al. 2020).

Due to fragile physical characteristics and the acceleration of human activities, the coastal mountain area (CMA) is considered one of the most vulnerable areas to geomorphological hazards in Syria (Alsafadi et al. 2022; Abdo 2018; Mohammed et al. 2020a, b, 2021). A literature review of geomorphological hazards in the eastern Mediterranean revealed an almost complete absence of studies related to landslide susceptibility in CMA which is prone to annual landslide events. For example, landslides in the winter of 2019 caused severe consequences regarding casualties and the partial destruction of the infrastructure in the Tartous Governorate. In this regard, the importance of this study can be justified by

Abdo *et al. Geoscience Letters*     (2022) 9:45

Page 3 of 24

the urgent need to conduct more landslide assessment studies in a highly vulnerable area such as CMA. In addition, the abundance of related spatial data is considered a significant challenge in light of the consequences of the current war in Syria and spatial data availability (Chaaban et al. 2022). Thus, bivariate statistical methods (BSM) provide a reliable assessment with constructive results, especially in areas with scarce data. Moreover, the relevant literature has demonstrated the flexibility and performance quality of BSM, especially in the Mediterranean mountain environment (Karim et al. 2019; Karaman et al. 2022; Akter and Javed 2022).

The main goals of the present assessment are: (1) to digitize the current landslide events; (2) to map landslide conditioning factors; (3) to map landslide susceptibility using frequency (FR), Statistical Index (SI) and index of entropy (IOE); and (4) to assess the accuracy performance and outputs. The major importance of this analysis is to conduct an accurate landslide susceptibility assessment for Al-Balouta river basin through the combination and comparison of those models. This study provides spatial insights of high importance to national planners in terms of landslide hazard managing landslide risk in the study area, especially during the current war period in Syria, which caused a great gap in relevant studies.

## Study area
The Al-Balouta river basin is sited in northwestern Syria, between Latitude 34° 57′–35° 04′ North and longitudes 36° 01′–36° 17′ East with an area of 116 km$^2$ (Fig. 1). This basin boarded by Al-Khawabi river basin to the west, Al-Ghab river basin to the west, Qays River basin to the south and Marqya River basin to the north. Geologically, the lithological structure of the study area varies from the Jurassic to the Quaternary (Ponikarov et al. 1967). Jurassic and Cretaceous formations consist of limestone, dolomite, marls, ophiolites, limy marl and sandy limestone. Neogene structure consists of basalt and sedimentary stones. Quaternary consists of *Pleistocene* and *Holocene* formations with fluviatile gravels, boulders, and deposits in riverbeds. The study area can be categorized into two major geomorphological regions based on the phase of terrestrial development (Abdo 2020). The hills area (110–400 m) consists of mainly upland parts distinguished by relatively sloping valleys. Dissected mountains area (400–1133 m) is featured faulted walls, steep slopes, narrow valleys and a diversity of geomorphological processes, especially karstification. The study basin is mainly subjected to the Mediterranean climate pattern: mild and rainy winter and long, dry and hot summer. The average summer temperature is 23.6° while in the winter is 10.3°. The annual precipitation is between 1000 and 1300 mm,

with maximum precipitation recorded of about 320 mm in January. The study area is located in a wet climate *Csa* according to the Köppen−Geiger climate classification (Beck et al. 2018; Mohammed et al. 2020a).

## Methodology
### Data
The assessment of landslide susceptibility was carried out in the study area based on a set of data from various sources (Fig. 2). Digital elevation model (DEM) obtained from shuttle radar topographic mission (SRTM) was used for mapping the topographical factors i.e., slope angle, slope aspect, curvature, plan curvature, profile curvature, elevation, streams and TWI. Fault and lithological structure data were acquired from the Ministry of Oil and Mineral Resources, Geology Directorate−Lattakia. Vegetation data was extracted from Landsat-8 OLI sensor satellite data collected from the United States Geological Survey (USGC). Rainfall data was collected from the Directorate of Meteorology, Tartous governorate. Road network data was obtained from the Ministry of Transport and Communications, Directorate of Transport and Public Roads. However, the details of the data sources have illustrated in Table 1. Figure 2 illustrated the methodology applied in this study.

### Landslide inventory map
The landslide inventory map generally represents current and historical landslide events of an assigned area using various data sources, including GPS-based fieldwork, previous reports, interviews with locals and satellite image interpretation (Eitvandi et al. 2022; Abu El-Magd et al. 2021; Ali et al. 2021, 2020; Abu El-Magd et al. 2021). The literature review reveals that a landslide inventory map can be generated either by collecting past evidence of different landslide patterns or using high-resolution satellite data combined with field surveys or by recognizing specific sites of landslide events in Google Earth by high-resolution satellite imageries. Conventionally, the inventory map was created using direct field investigation to confirm the actual locations. However, at present with the development of spatial technology, this task turns out to be easier to obtain accurate and rapid results (Chen et al. 2017a; Ali et al. 2020; Sachdeva et al. 2020; Pham et al. 2021b). It is frequently suggested that equivalent numbers of non-landslide locations should also be chosen for preparation and validation (Chen et al. 2017b; Abu El-Magd et al. 2021; Ali et al. 2021). In the current study, the inventory map was prepared according to the following strategy: (1) create a preliminary inventory map derived from fieldwork, information from local authorities and interviews with locals, (2) use high-resolution images (interpretation of Google Earth images (Google
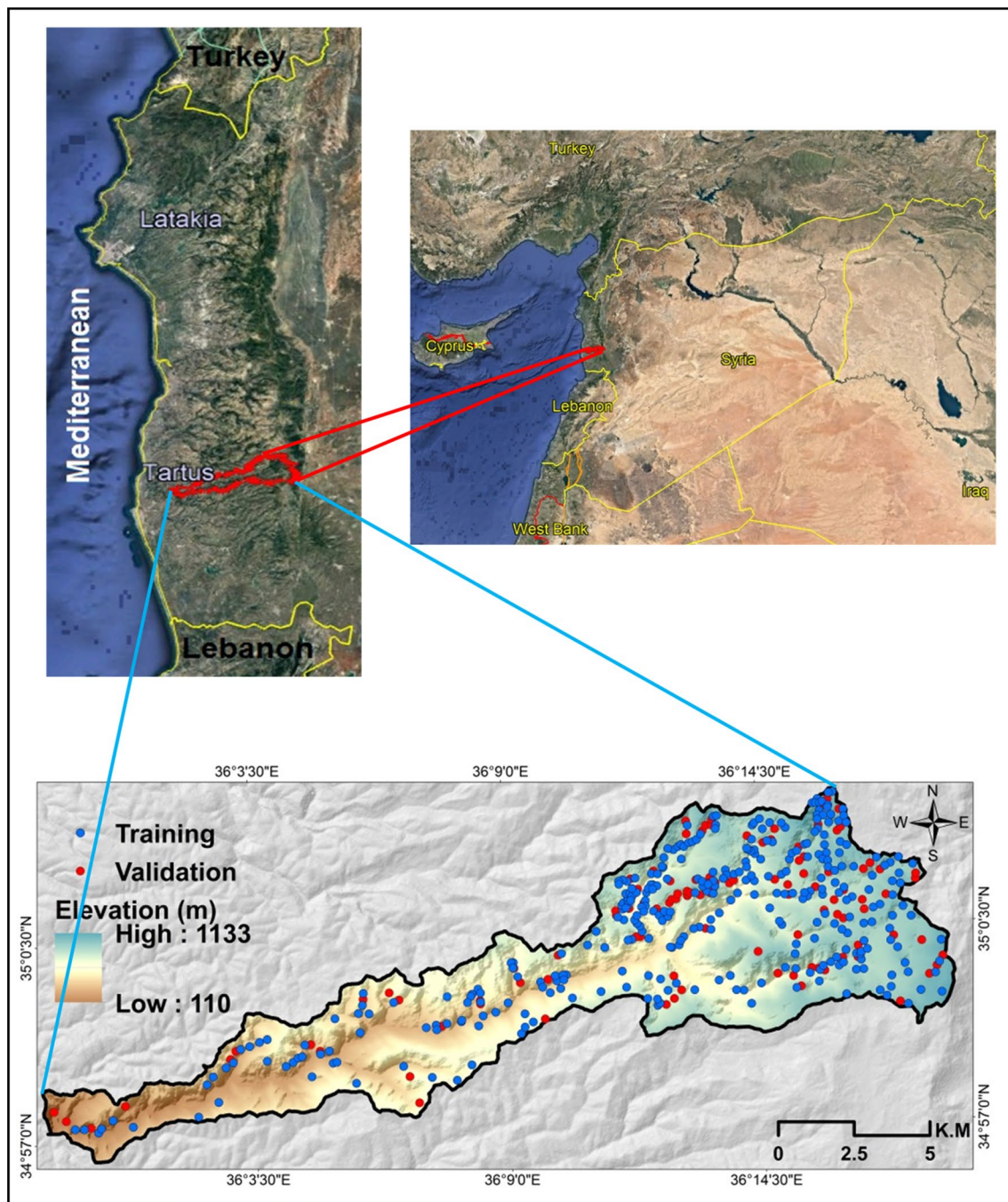
**Fig. 1** Location of the study area

Earth Pro tools) to complete the digitizing of landslide events, (3) verify the final inventory map quality by conducting extensive fieldwork in various parts of the basin. This strategy was relied upon due to the lack of national inventory maps that could assist in conducting landslide assessment studies. Thus, this strategy can be used in other areas of CMA. However, the Geostatistical Analyst

tools in ArcGIS (Geostatistical Analyst–Subset features) were used to divide the landslide events into a training dataset and a test dataset (Zhu et al. 2021; He et al. 2021; Pham et al. 2021a, b). A total of 446 locations of landslide events, however, are determined in study area. In this context, 70% (312 events) of landslides were selected randomly for the training dataset, whereas the rest of

Abdo *et al. Geoscience Letters*     (2022) 9:45

Page 5 of 24
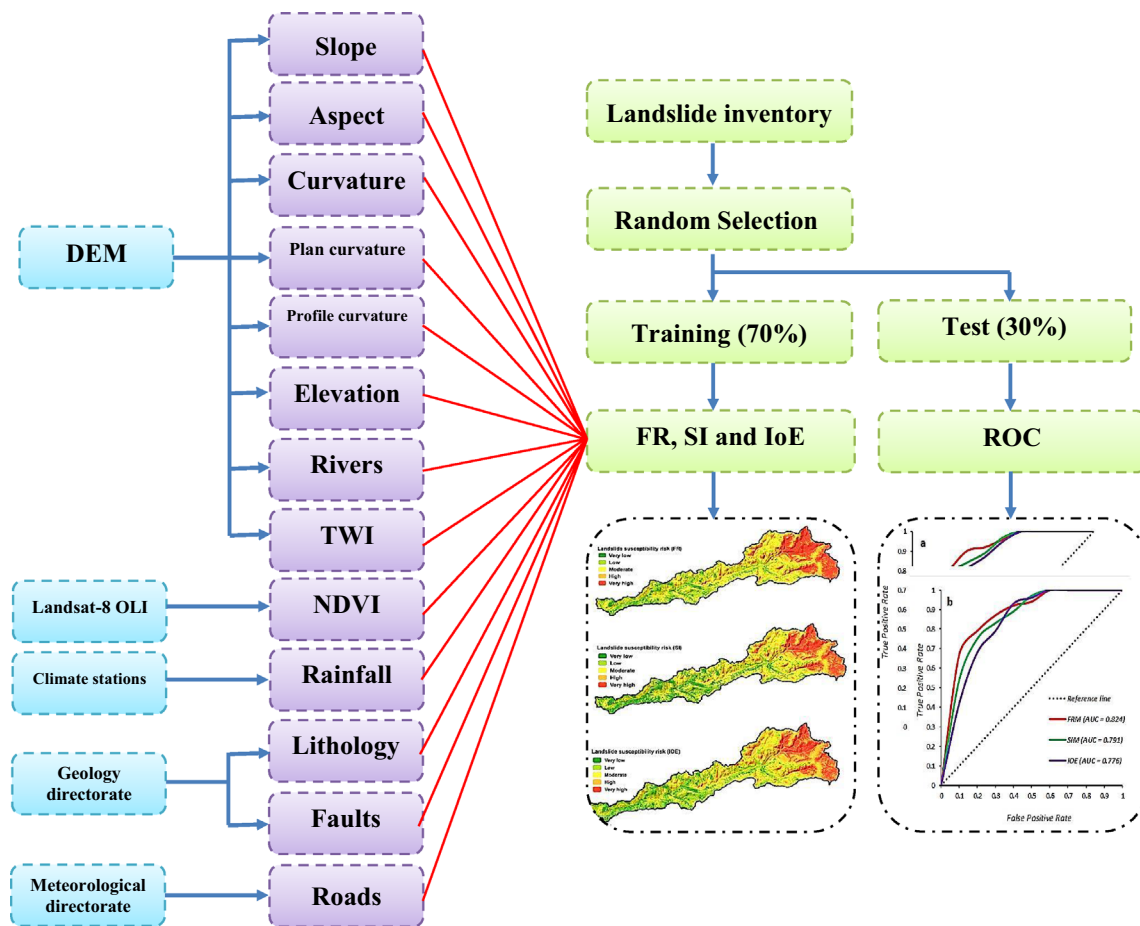


**Fig. 2** Flowchart of the applied methodology

**Table 1** Description and source of data used

| Factor | Data source | Format | Spatial resolution (m) | Source |
|---|---|---|---|---|
| Slope angle, slope aspect, curvature, plan curvature, profile curvature, elevation, streams, TWI | DEM | Raster | 30 | Shuttle Radar Topography Mission (SRTM) http://earthexplorer.usgs.gov/ |
| Faults and lithology | Geological maps of Tartous and Safita 1/50,000 | Polygon and line vector | – | Ministry of Oil and Mineral Resources (Geology Directorate-Lattakia) |
| Rainfall | Data of four climate stations | – | – | Directorate of Meteorology in Tartous governorate |
| NDVI | Landsat-8 OLI (April 16, 2020) | Raster | 30 | Landsat-8 OLI sensor satellite data https://earthexplorer.usgs.gov/ |
| Roads | Roads shepfile | Line vector | – | Ministry of Transport and Communications (Directorate of Transport and Public Roads) |

30% (134 events) data was utilized for model validation (Fig. 1). The fieldwork revealed the diversity of patterns and types of landslides as a result of the complex integration between the driving geographical characteristics in the study area (Table 2).

**Table 2** Detail information about landslide events

| Study area | Triggering spatial characteristics | Landslide type |
|---|---|---|
| Upper basin | Fragile lithological structure of dolomite and limestone, dense faults, very steep slopes, high rainfall intensities, dense vegetation and accelerated karstification process | Rainfall-induced rapid mass movements, rock falling, bouncing and rolling |
| Middle basin | Fragile lithological structure of marl, dolomite and limestone, dense faults, steep slopes, high rainfall intensity, dense vegetation, accelerated karst decomposition process and human activity including urbanization, infrastructure projects, dense slope cultivation and tourism activity | Rock falls and sliding and debris and mud flows |
| Lower basin | Fragile lithological structure of limestone and sandstone, gentle slopes, moderate rainfall intensities and human activity including urban expansion, infrastructure projects, floodplain farming and tourism activity | Shallow landslides and debris and mud flows |

## Landslide susceptibility index

### Frequency ratio (FR)

The frequency ratio is one of the well-known and widely used BSM which have been frequently applied for hazard susceptibility mappings, such as flood and landslide (Ali et al. 2020; Kincal and Kayhan 2022). FR is a widely utilized method for understanding the potential linking between current landslide events and causative geofactors (Rahman et al. 2022). However, FR can be defined through a spatial relationship between dependent and independent variables, where landslide inventory is the dependent variable and landslide conditioning factors are the independent variable. The weight of frequency ratio was estimated by dividing the pixels containing landslide points in each conditioning factors class and the total pixels of the considered area. The final weight in the frequency ratio for each conditioning factor is estimated using the following equation (Eq. 1):

$$FR = \frac{\left( Xpixel_{Li} / Ypixel_{Ti} \right)}{\left( \sum Xpixel_{Li} / \sum Ypixel_{Ti} \right)} \quad (1)$$

where $Xpixel_{Li}$ is No. of pixels containing landslide points in class X, $Ypixel_{Ti}$ is the No. of total pixels covering in class X over the study area, $\sum Xpixel_{Li}$ is the sum of pixels containing landslide points in class X and $\sum Ypixel_{Ti}$ is the sum of pixels covering in class X over the study area.

The value of frequency ratio >1 indicates there is a positive relationship between training points and each class of landslide conditioning factor and high landslide susceptibility, whereas a value <1 directs negative relation and low landslide susceptibility (Mind'je et al. 2020).

### Statistical index (SI)

A statistical index (SI) is also BSM commonly used for landslide susceptibility assessment (Thapa and Esaki 1970). Using the SI, the particular class of a conditioning factor can be weighted based on the pixel concentration of landslide points of specific criteria and the total pixel concentration of landslide points across the whole study area (Bourenane et al. 2021). The weight of landslide factors computed using SI can be expressed as Eq. (2)

$$SI = In\left( \frac{ld_{ij}}{td} \right) = In\left( \frac{\frac{L_{ij}}{L_{tn}}}{\frac{pix_{ij}}{pix_t}} \right) \quad (2)$$

where $ld_{ij}$ is the landslide density for $i$ class of $j$ factor, td is the total landslide density of the whole study region, $L_{ij}$ is the number of landslides in $i$ class of $j$ factor, $L_{tn}$ is the total number of landslides in the whole study region, $pix_{ij}$ is the number of pixels in $i$ class of $j$ factor, and $pix_t$ is the total pixels of the whole study region.

The positive and negative value calculated using SI shows the presence and absence of a link between each class of landslide causative factors and landslide current events of landslide, respectively (Razavizadeh et al. 2017).

### Index of entropy (IoE)

Index of entropy (IOE) is another BSM used for landslide susceptibility mapping, where determined on the basis of certain variables which calculate the weight of each variable. In this method, entropy depicts the level of uncertainty, imbalance, disorder and instability (Youssef et al. 2015). The role of different conditioning factors on the occurrence of landslides is represented by the entropy which provides an index system (Sahana et al. 2020) So, the value of entropy is useful for calculating the factor's weight (Zhang et al. 2019). The equations which are used for calculating the information coefficient and $W_f$ expressing the weight of factors as a whole are as follows (Eqs. 3–8)

$$P_{rs} = \frac{p}{q} \quad (3)$$

$$(P_{rs}) = P_{rs} \Big/ \sum_{s=1}^{L_s} P_{rs} \quad (4)$$

Abdo *et al. Geoscience Letters*      (2022) 9:45

Page 7 of 24

$$E_s = \sum_{s=1}^{L_s} (P_{rs}) \log_2 (P_{rs}), s = 1, \ldots, n \qquad (5)$$

$$E_{\mathrm{smax}} = \log_2 L_s, L_s - \mathrm{No.\,of\ classes} \qquad (6)$$

$$I_s = E_{\mathrm{smax}} - E_s \big/ E_{s\,\mathrm{max}}, I = (0,1), s = 1, \ldots\ldots, n \quad (7)$$

$$W_f = I_s P_{rs} \qquad (8)$$

where $p$ and $q$ are the area and percentage of landslide, respectively, $P_{rs}$ is the density of possibility, $E_s$ and $E_{\mathrm{smax}}$ are the entropy values, $I_s$ and $W_f$ are information coefficient and factor's weight as a whole, respectively.

## Results

### Landslide-controlling criteria

A landslide is a physical phenomenon that occurs due to the synergic action of many environmental factors (Dikshit et al. 2020). Therefore, to accurately estimate the spatial risk of landslides, it is very critical to select the triggering factors which have a high influence on the landslides. However, it should be noted that these were selected depending on the initial data availability, type and pattern of landslides, geographical features of the study area and Mediterranean landslide literature (Yu et al. 2022; Senouci et al. 2021; Ullah et al. 2022). At the present assessment, 13 landslide conditioning factors were selected (i.e. slope degrees, slope aspect, curvature, plan curvature, profile curvature, altitude, distance from faults, distance from streams, distance from roads, Normalized Difference Vegetation Index (NDVI), precipitation, geology and Topographic Wetness Index (TWI).

### Slope angle

Slope angle is a main terrestrial motivating factor influencing slope debris stabilization (Costache and Tien Bui 2020; Abdo 2022). It is an important landslide conditioning factor because the likelihood of landslide occurrence increases with the slope angle values (Abedini et al. 2019). Mohan et al. (2021) mentioned that the effects of stress and gravity on the slope materials are higher with the slope angle increasing. In the current evaluation, the slope angle parameter map of the study basin was derived from digital elevation model (DEM) and was divided into six classes: flat (0°–5°), gentle slope (5°–10°), moderate (10°–15°), moderate steep (15°–20°), steep (20°–25°) and very steep (<25°) as reported in Fig. 3a.

### Slope aspect

Slope aspect has an indirect influence on landslide triggering because it could control some of the climatic parameters like humidity, insolation, wind speed and direction, amount of precipitation, etc (Abdo 2021; Ma et al. 2020). Aspect map, moreover, indicates how much the proportion of the investigated area is covered with various slope directions. In the present assessment, the slope aspect parameter map was also derived from the DEM and is characterized by 8 aspect directions and the flat zones: as flat (− 1), north (337.5°–360°, 0°–22.5°), northeast (22.5°–67.5°), east (67.5°–112.5°), southeast (112.5°–157.5°), south (157.5°–202.5°), southwest (202.5°–247.5°), west (247.5°–292.5°) and northwest (292.5°–337.5°) as illustrated in Fig. 3b.
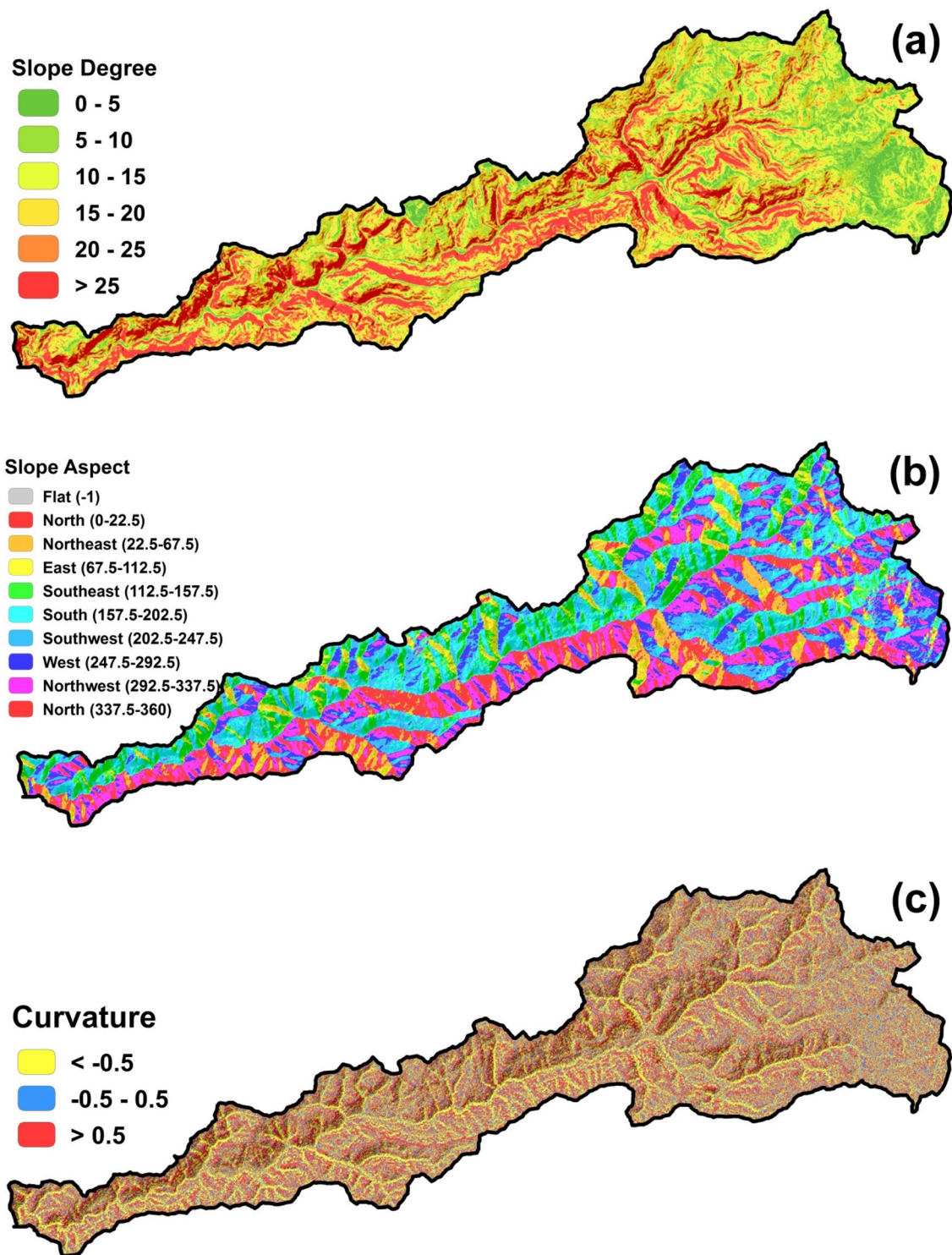
### Curvature

Curvature represents another morphometric landslide predictor, derived from DEM, which has a high influence on landslide susceptibility by shifting the values of slope angle or aspect. Curvature effects throw given by the control that the values of the curvature have over the phenomenon of soil erosion and the rapid flow of water on the slopes (Costache and Tien Bui 2020). In this regard, negative curvature shows an area of land that is concave, while a positive curvature highlights a convex surface of the ground. In this assessment, the values of the curvature were divided into the following classes: <− 0.05 (negative curvatures), − 0.05–0.05 (flat) and >0.05 (positive curvatures) as shown in Fig. 3c.

### Plan curvature

The plan curvature, which is derived also from DEM in GIS environment, is an important landslide conditioning factor because its values can indicate the areas with a convergent or a divergent runoff (Costache and Tien Bui 2020) Plan curvature affects the dramatic change of water channels distance by the slope flowing (Ullah et al. 2022). Figure 3d shows the plan curvature map that was extracted from the DEM in GIS environment and categorised into three groups: <− 0.05 (negative plan curvatures), − 0.05–0.05 (flat) and >0.05 (positive plan curvatures) as presented in Fig. 3d.

### Profile curvature

Profile curvature is an important morphometric landslide influencing factor because it shows the areas with accelerated soil erosion and runoff (Costache 2019). Thus, profile curvature essentially triggered the slope debris movement (Di et al. 2019) Profile curvature values in this study were calculated by using DEM in GIS environment and classified in the following classes <− 0.05 (negative plan curvatures), − 0.05–0.05 (flat) and >0.05 (positive plan curvatures) as showed in Fig. 3e.

Abdo *et al. Geoscience Letters*     (2022) 9:45

Page 8 of 24



**Fig. 3** Spatial outputs for delanating landslide sensitivity maps of Al-Balouta river basin **a** slope angels, **b** slope aspect, **c** curvature, **d** profile curvature, **e** plan curvature, **f** altitude, **g** NDVI, **h** proximity to faults, **i** proximity to rivers, **j** proximity to roads, **k** rainfall, **l** lithology and **m** TWI
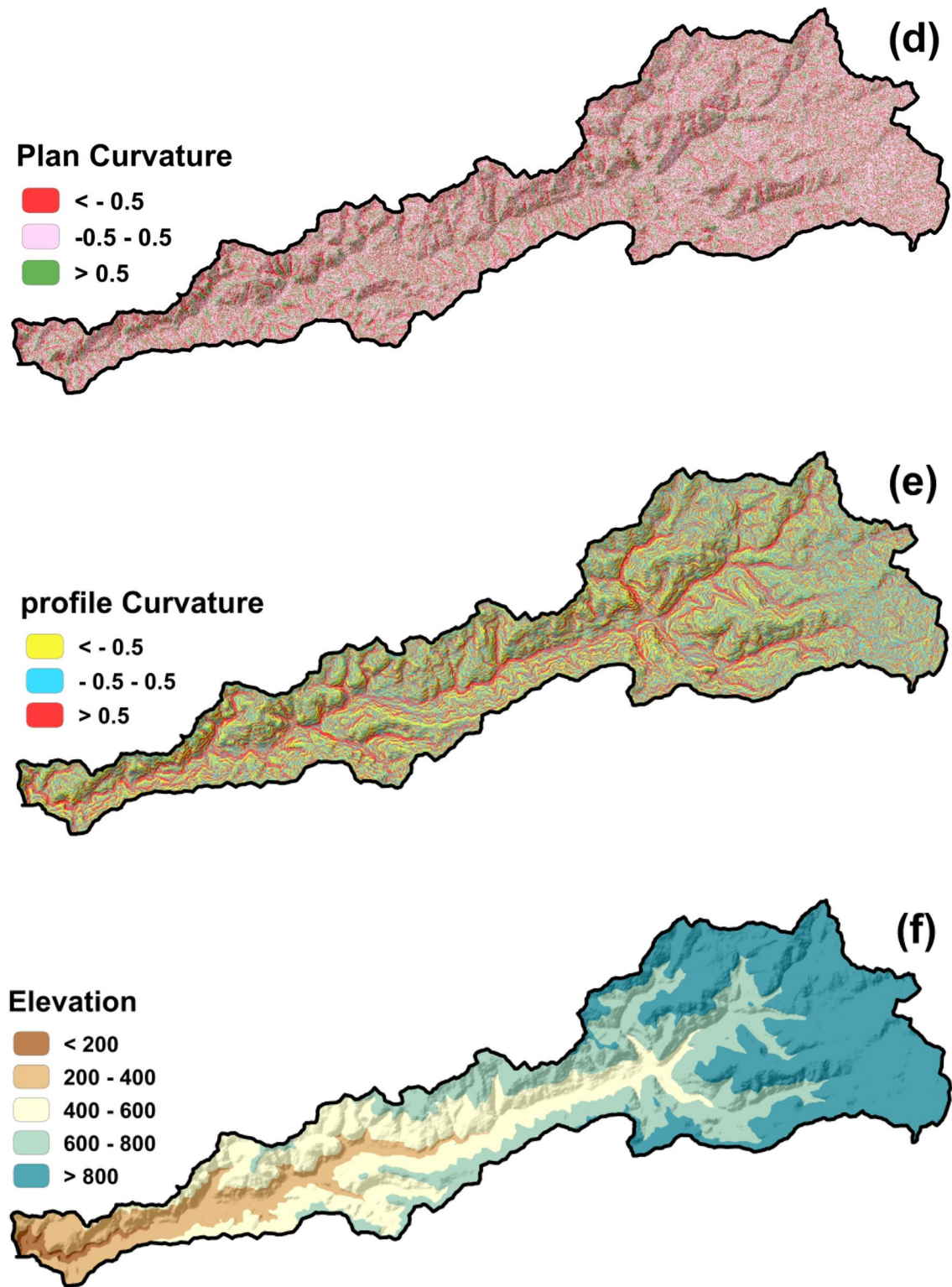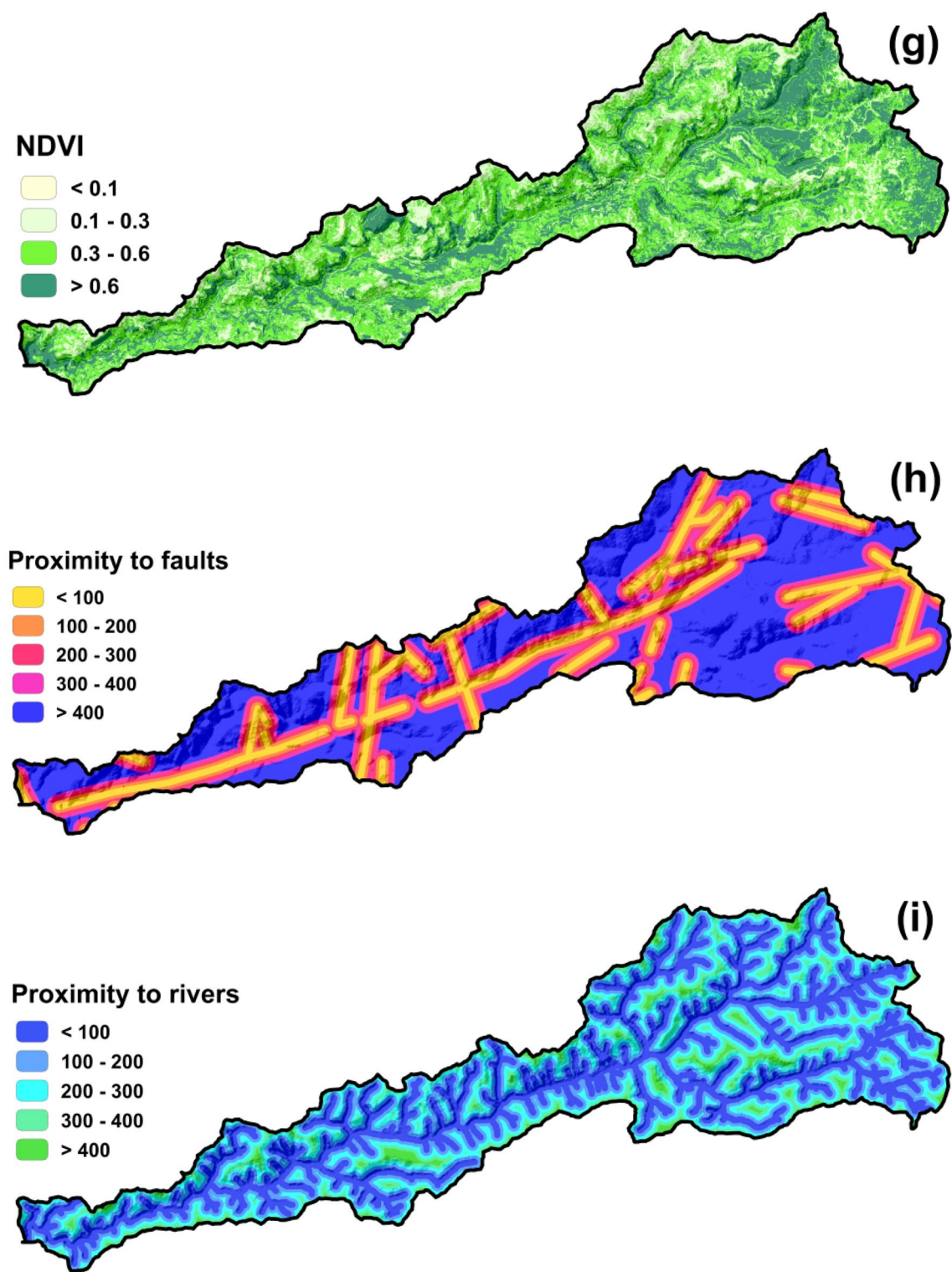
Abdo *et al. Geoscience Letters* (2022) 9:45

Page 9 of 24



**Fig. 3** continued

**Fig. 3** continued

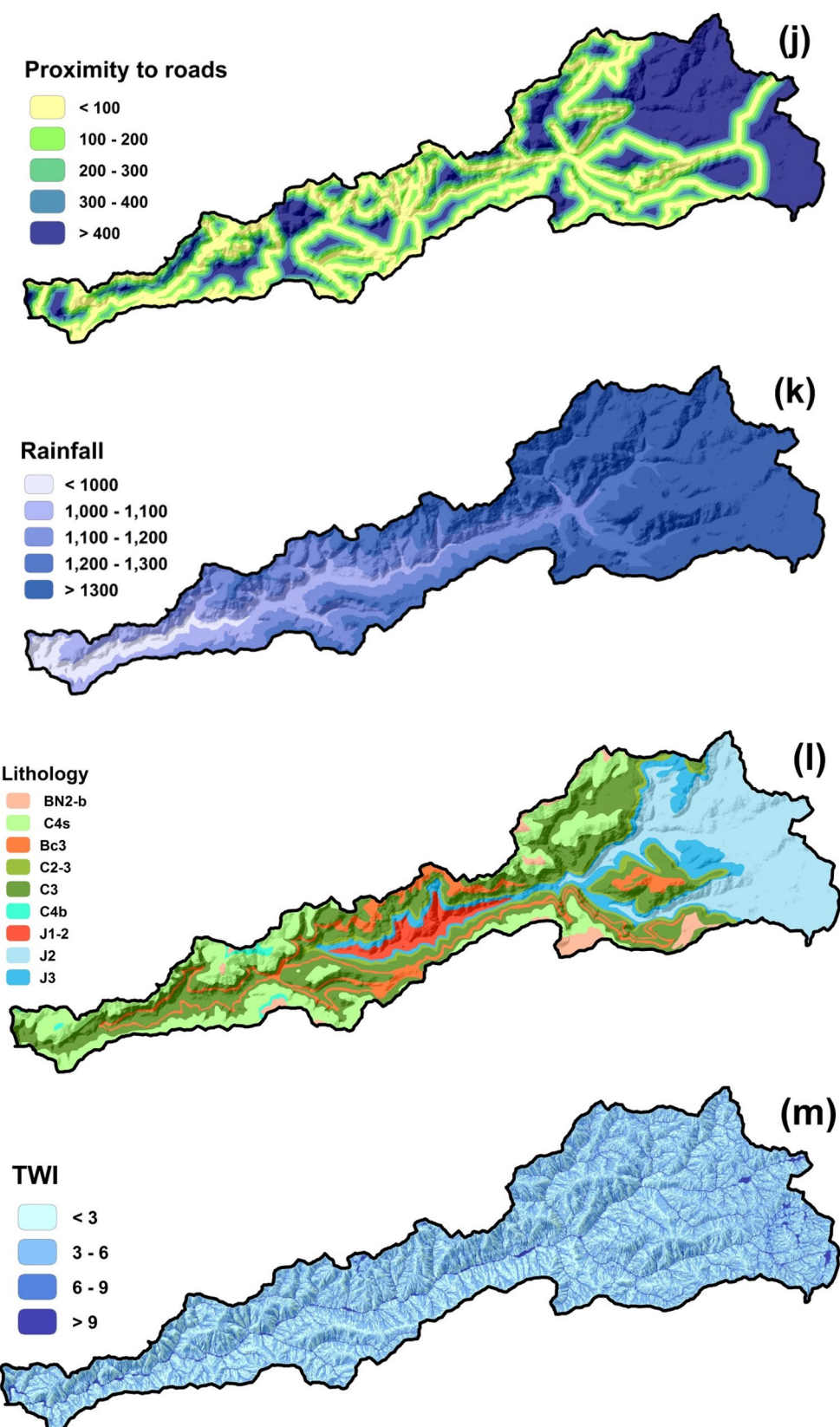Abdo *et al. Geoscience Letters*     (2022) 9:45

Page 11 of 24



**Fig. 3** continued

### Elevation

The elevation conditioning factor is a highly used parameter in landslide susceptibility studies due to the fact that this factor controls many other climatic as well as geomorphological parameters (Costache and Tien Bui 2020). It is often considered that the susceptibility to landslides is higher in areas with high altitudes and vice versa (Chen et al. 2018; Costache and Tien Bui 2020). In this study, the elevation factor map was extracted using DEM and divided into five classes: <200 m, 200–400 m, 400–600 m, 600–800 m and >800 m as shown in Fig. 3f.

### Proximity to faults

The proximity to faults is an essential geological factor triggering landslide sensitivity since the likelihood of landslides will increase as the distance to faults decreases (Fang et al. 2021). Primarily, the landslide phenomenon will occur along the faults that enhance slope instability. The proximity to faults map, in the current evaluation, was calculated using the *Euclidean Distance* tool in GIS software as shown in Fig. 3g.

### Proximity to rivers

Similar to the case of the previous factor, the proximity to rivers is a significant triggering criterion for landslide susceptibility (Ma et al. 2020). In fact, a watercourse can destabilize the stabilization of the slope by flow energy and erosion capacity, especially down the slope (Sahana et al. 2020). In the case of the current investigation, the proximity to rivers was grouped into five classes as shown in Fig. 3h.

### Proximity to roads

The proximity to roads is an anthropogenic factor that influences directly triggers slope materials instability (Karlsson et al. 2017). The road construction process and the weight and traffic of vehicles could frequently lead to landslide occurrence. The road network was derived from the Directorate of Transportation of Tartous Governorate (DTTG) and buffered with a *Euclidean distance* of 100 m in the GIS environment to paper the proximity to the road map (Fig. 3i).

### NDVI

The Normalized Difference Vegetation Index (NDVI) is a wide landslide conditioning factor used in the majority of the previous landslide assessment literature (Hussain et al. 2022; Yousefi et al. 2022; Huang and Zhao 2018; Wu et al. 2020). NDVI map was created by utilizing Landsat 8 imagery and Eq. 9:

$$NDVI = (NIR - RED)/(NIR + RED) \qquad (9)$$

where NIR is the near-infrared band (band 4, 0.76–0.90 μm) and RED is the red band (band 3, 0.63–0.69 μm). Figure 3j showed the classes of NDVI values in the study area.

### Rainfall

Rainfall is a principal climatic criterion that motivates slope materials instability by the heavy rainfall intensifications, the high kinetic energy of the raindrops and generated runoff (Youssef et al. 2015; Bui et al. 2019; Sahana et al. 2020). In this regard, landslide events accelerate in the Mediterranean mountainous regions due to the orographic precipitation pattern which produces heavy rainstorms with great peaks of runoff (Mohammed et al. 2020a). The rainfall map in the study area was delineated depending on the five rainfall stations data (1972–2019) obtained from the Directorate of Meteorology in Tartous governorate. The inverse distance weighted (IDW) method, however, was utilized for mapping (Mohammed et al. 2020a; Valiante et al. 2021). Figure 3k depicted the five spatial domains of rainfall: >1000 mm, 1000–1100 mm, 1100–1200 mm, 1200–1300 mm and >1300 mm.

### Lithology

Lithology is a landslide conditioning factor that can provide very useful information regarding the likelihood of landslide occurrence based on the structural features of specific geological formations (Abedini et al. 2019). For example, the presence of specific rock clays or marl can favour landslide occurrence (Sahana et al. 2020). Nine geological entities in the study area were digitized from Tartous, Safita and Mesiyaf geological map 1:50,000, including *Upper Jurassic* (J3), *Middel Jurassic* (J2), *Lower Jurassic* (J1), *Albian and Abitian* (C2-3), *Lower Albian* (C2), *Lower Cenomanian* ($C_4^s$), *Upper Cenomanian* ($C_4^b$), *Basaltic Albian* ($B_c^3$) and *Basaltic Paleocene* ($\beta N_2$-b), as illustrated in Fig. 3l.

### TWI

Topographic Wetness Index (TWI) is a morphometrical indicator commonly used in recent studies related to landslide susceptibility mapping. TWI values highlight the areas where the topographical humidity is higher due to high water accumulation (Singha et al. 2022; Chen et al. 2018; Abdo 2020). TWI is calculated utilizing DEM in GIS environment based on Eq. (10).

$$TWI = \ln\left(\frac{\alpha}{\tan\beta}\right) \qquad (10)$$

where $\alpha$ is the cumulative up slope area draining through a point (per unit contour length) and $\tan\beta$ is the slope

angle at the point. In the present assessment, the TWI values were divided into four spatial domains as:<3) low wetness), 3–6 (moderate wetness), 6–9 (high wetness) and >9 (very high wetness), as shown in Fig. 3m.

### Landslides correlation with conditioning criteria
#### *Application of FR*
As per the equation of FR (Eq. 1), if the value is >1, it signifies that there is a positive correlation between training points and a particular class of landslide conditioning factors and high landslide susceptibility. The result of the FR model showed that the slope with 20°–25° and >25° have a ratio value of 1.31 and 1.26, respectively. The slope aspect facing east, southeast and south, all have a ratio value >1. Convex curvature with ratio value 1.12, 600–800 m and >800 m elevation with ratio value 1.22 and 1.23, respectively, NDVI ranges between 0.3 and 0.6 with a ratio value 1.19, proximity to a fault between 100 and 200 m with a ratio value of 1.07, proximity to rivers between 100 and 200 m and <100 m with ratio value 1.33 and 1.11, respectively, rainfall >1300 with 1.33 ratio value, among lithology J2 and J1-2 with ratio value 1.81 and 1.82, respectively and greater value of TWI (>9) has a ratio value 1.07, indicating that these all are a more relevant class of the selected criteria having a significant role in landside occurring and positive correlation with landslide susceptibility (Table 3).

#### *Application of SI*
In the case of a SI, a positive and negative value of each class of landslide conditioning factors indicates the presence and absence of a relationship with landslide susceptibility. The result of SI is more similar to FR. Table 3 shows that those classes of landslide conditioning factors have an FR value of >1, having a positive SI value. The result of the calculated SI value shows that the slope is between 20° and 25° and >25° have SI values of 0.27 and 0.23, respectively. Slope aspect facing east (SI=0.08), southeast (SI=0.52) and south (SI=0.32), all have a positive value. Convex curvature (SI=0.11), elevation with 600–800 m and >800 m (SI=0.20 and 021, respectively), NDVI ranges between 0.3 and 0.6 (SI=0.18), proximity to a fault between 100 and 200 m (SI=0.07), proximity to river between 100 and 200 m and <100 m (SI=0.28 and 010, respectively), rainfall >1300 (SI=0.32), among lithology J2 and J1-2 (SI=0.59 and 0.60, respectively) and the value of TWI with >9 (SI=0.07), representing important classes causing landslides in the stud area.

#### *Application of IoE*
Based on Eqs. (3–8), the individual factor's weight has been calculated for preparing the landslide susceptibility index. A higher value of the index of entropy (IOE)

indicates more causative for landslide occurring. The result of IOE weight reveals that proximity to faults, lithology and proximity to roads having an IOE value of 1.26, 1.22 and 1.19, respectively, followed by proximity to river (IOE=0.99), rainfall (IOE=0.91) and TWI (IOE=0.74). Hence, these are more important factors for evaluating landslide susceptibility in the study area out of the thirteen selected. On the other hand, curvature (IOE=0.004), plan curvature (IOE=0.01), slope (IOE=0.02), profile curvature (IOE=0.04), elevation (IOE=0.04) and slope aspect (IOE=0.07) are less important factors for landslide susceptibility assessment in the study area with lower IOE value (Table 4).

### Landslide delineation and assessment
In this analysis, three different statistical approaches were tested in modelling the landslide susceptibility in Al-Balouta river basin. In this regard, data derived from augmented fieldwork and remote sensing in a GIS environment were used in the modelling process. Figures 4, 5 and 6 show the results of the multi-criteria modelling process after being categorized using the *Natural Brecks* method in a GIS environment into five degrees of severity: very low, low, moderate, high and very high.

Moreover, Fig. 7 indicates the classification of landslide pixels for each susceptibility degree in the study area. In the FR-based modelling, 18.51% and 19.98% of the study area fall under high and very high landslide susceptibility, respectively. While moderate, low and very low covered 29.09%, 24.63% and 7.78% of the area under investigation, respectively. In the map generated by the SI method, about 36% of the study area is classified under high and very high landslide sensitivity. Whilst, the remaining 25%, 23.57% and 15.30% of landslides are classified as moderate, high and very high landslide susceptibility, respectively. In the IOE method, 14.18% and 25.62% of the study area were classified as very high and high landslide susceptible, respectively. While moderate, low and very low landslide susceptibility covered 19.87%, 30.04% and 10.29% of the study area, respectively.

### Validation of landslides susceptibility map
Landslide vulnerability prediction maps are among the most important tools for managing natural hazards associated with slope stability in river basins. Statistical models that spatially linking between landslide incidents and causative factors provide a reliable and constructive approach in the landslide sensitivity mapping process. However, evaluating the accuracy of the conducted modelling process outputs is a necessary final procedure in order to verify the applied models performance. At the present study, landslide capability maps acquired by the FR, SI and IOE were evaluated using the verifying data

**Table 3** The linking between classes of landslide causative criteria and present landslide events by FR

|    | Parameter | Class | No. of landslide | % of landslide | No. of pixels in domain | % of domain | FR | SI |
|----|-----------|-------|------------------|----------------|-------------------------|-------------|------|------|
| 1  | Slope (Degree) | 0–5 | 12 | 3.59 | 43,627 | 5.86 | 0.61 | − 0.49 |
|    |           | 5–10 | 41 | 12.28 | 119,918 | 16.10 | 0.76 | − 0.27 |
|    |           | 10–15 | 71 | 21.26 | 163,382 | 21.93 | 0.97 | − 0.03 |
|    |           | 15–20 | 71 | 21.26 | 175,950 | 23.62 | 0.90 | − 0.11 |
|    |           | 20–25 | 71 | 21.26 | 121,309 | 16.28 | 1.31 | 0.27 |
|    |           | 25< | 68 | 20.36 | 120,811 | 16.22 | 1.26 | 0.23 |
| 2  | Slope aspect | Flat | 0 | 0.00 | 1308 | 0.18 | 0.00 | None |
|    |           | North | 9 | 2.69 | 52,881 | 7.10 | 0.38 | − 0.97 |
|    |           | Northeast | 13 | 3.89 | 56,363 | 7.57 | 0.51 | − 0.66 |
|    |           | East | 22 | 6.59 | 45,126 | 6.06 | 1.09 | 0.08 |
|    |           | Southeast | 75 | 22.46 | 99,730 | 13.39 | 1.68 | 0.52 |
|    |           | South | 84 | 25.15 | 136,654 | 18.34 | 1.37 | 0.32 |
|    |           | Southwest | 41 | 12.28 | 98,417 | 13.21 | 0.93 | − 0.07 |
|    |           | West | 35 | 10.48 | 92,398 | 12.40 | 0.84 | − 0.17 |
|    |           | Northwest | 38 | 11.38 | 110,164 | 14.79 | 0.77 | − 0.26 |
|    |           | North | 17 | 5.09 | 51,956 | 6.97 | 0.73 | − 0.31 |
| 3  | Curvatuer | Concave | 112 | 33.53 | 280,770 | 37.69 | 0.89 | − 0.12 |
|    |           | Flat | 79 | 23.65 | 179,517 | 24.10 | 0.98 | − 0.02 |
|    |           | Convex | 143 | 42.81 | 284,710 | 38.22 | 1.12 | 0.11 |
| 4  | Plan curvature | Concave | 89 | 26.65 | 235,248 | 31.58 | 0.84 | − 0.17 |
|    |           | Flat | 111 | 33.23 | 264,520 | 35.51 | 0.94 | − 0.07 |
|    |           | Convex | 134 | 40.12 | 245,229 | 32.92 | 1.22 | 0.20 |
| 5  | Profile curvature | Concave | 122 | 36.52 | 248,078 | 33.30 | 1.10 | 0.09 |
|    |           | Flat | 118 | 35.32 | 250,650 | 33.64 | 1.05 | 0.05 |
|    |           | Convex | 94 | 28.14 | 246,269 | 33.06 | 0.85 | − 0.16 |
| 6  | Elevation | <200 | 3 | 0.89 | 8707 | 1.17 | 0.77 | − 0.26 |
|    |           | 200–400 | 16 | 4.79 | 85,598 | 11.49 | 0.42 | − 0.87 |
|    |           | 400–600 | 55 | 16.46 | 177,848 | 23.87 | 0.69 | − 0.37 |
|    |           | 600–800 | 106 | 31.73 | 193,667 | 26.00 | 1.22 | 0.20 |
|    |           | >800 | 154 | 46.10 | 279,177 | 37.47 | 1.23 | 0.21 |
| 7  | NDVI | <0.1 | 1 | 0.299 | 4402 | 0.59 | 0.51 | − 0.68 |
|    |           | 0.1–0.3 | 21 | 6.28 | 133,083 | 17.86 | 0.35 | − 1.04 |
|    |           | 0.3–0.6 | 201 | 60.18 | 375,287 | 50.37 | 1.19 | 0.18 |
|    |           | >0.6 | 111 | 33.23 | 232,225 | 31.17 | 1.07 | 0.06 |
| 8  | Proximity to faults | <100 | 44 | 13.17 | 101,919 | 13.68 | 0.96 | − 0.04 |
|    |           | 100–200 | 47 | 14.07 | 97,725 | 13.12 | 1.07 | 0.07 |
|    |           | 200–300 | 39 | 11.67 | 90,056 | 12.09 | 0.97 | − 0.03 |
|    |           | 300–400 | 28 | 8.38 | 81,158 | 10.89 | 0.77 | − 0.26 |
|    |           | >400 | 176 | 52.69 | 374,139 | 50.22 | 1.05 | 0.05 |
| 9  | Proximity to rivers | <100 | 130 | 38.92 | 261,091 | 35.05 | 1.11 | 0.10 |
|    |           | 100–200 | 127 | 38.02 | 213,740 | 28.69 | 1.33 | 0.28 |
|    |           | 200–300 | 52 | 15.56 | 161,657 | 21.70 | 0.72 | − 0.33 |
|    |           | 300–400 | 20 | 5.98 | 85,007 | 11.41 | 0.52 | − 0.64 |
|    |           | >400 | 5 | 1.49 | 23,502 | 3.15 | 0.47 | − 0.75 |
| 10 | Proximity to roads | <100 | 42 | 12.57 | 210,599 | 28.27 | 0.44 | − 0.81 |
|    |           | 100–200 | 49 | 14.67 | 149,672 | 20.09 | 0.73 | − 0.31 |
|    |           | 200–300 | 39 | 11.67 | 104,913 | 14.08 | 0.83 | − 0.19 |
|    |           | 300–400 | 45 | 13.47 | 70,282 | 9.43 | 1.43 | 0.36 |
|    |           | >400 | 159 | 47.60 | 209,531 | 28.13 | 1.69 | 0.53 |

**Table 3** (continued)

|  | Parameter | Class | No. of landslide | % of landslide | No. of pixels in domain | % of domain | FR | SI |
|---|---|---|---|---|---|---|---|---|
| 11 | Rainfall | <1000 | 6 | 1.796 | 32,050 | 4.30 | 0.42 | − 0.87 |
|  |  | 1000–1100 | 23 | 6.88 | 78,308 | 10.51 | 0.66 | − 0.42 |
|  |  | 1100–1200 | 41 | 12.27 | 136,634 | 18.34 | 0.67 | − 0.40 |
|  |  | 1200–1300 | 44 | 13.17 | 141,577 | 19.00 | 0.69 | − 0.37 |
|  |  | >1300 | 220 | 65.86 | 356,428 | 47.84 | 1.38 | 0.32 |
| 12 | Lithology | C2-3 | 6 | 1.7 | 32,186 | 4.32 | 0.42 | − 0.88 |
|  |  | J3 | 24 | 7.18 | 63,649 | 8.54 | 0.84 | − 0.17 |
|  |  | C3 | 85 | 25.44 | 221,036 | 29.67 | 0.86 | − 0.15 |
|  |  | Bc3 | 6 | 1.79 | 55,183 | 7.41 | 0.24 | − 1.42 |
|  |  | BN2-b | 1 | 0.29 | 21,363 | 2.87 | 0.10 | − 2.26 |
|  |  | C4s | 47 | 14.07 | 143,762 | 19.30 | 0.73 | − 0.32 |
|  |  | C4b | 0 | 0 | 4313 | 0.58 | 0.00 | None |
|  |  | J2 | 146 | 43.71 | 180,214 | 24.19 | 1.81 | 0.59 |
|  |  | J1-2 | 19 | 5.68 | 23,291 | 3.13 | 1.82 | 0.60 |
| 13 | TWI | <3 | 292 | 87.42 | 619,173 | 83.11 | 1.05 | 0.05 |
|  |  | 3–6 | 35 | 10.47 | 101,664 | 13.65 | 0.77 | − 0.26 |
|  |  | 6–9 | 3 | 0.89 | 15,841 | 2.13 | 0.42 | − 0.86 |
|  |  | >9 | 4 | 1.19 | 8319 | 1.12 | 1.07 | 0.07 |

sets excluded from the modelling process. The area under curve (AUC) of the receiver-operating characteristics (ROC) was utilized for the standard accuracy evaluation of both landslide sensitivity outputs and the three models performance. The forecasting rate curves (Fig. 8a) showed that the applied models performance in landslide susceptibility modelling is greater for FR with 0.841 of AUC followed by SI and IOE with 0.821 and 0.788 of AUC, respectively. Moreover, Fig. 8b illustrated that the AUC of performed models success rate was larger for FR with 0.824, followed by SI and IOE with 0.791 and 0.776 of AUC. In this sense, prior validation outcomes illustrate that the used curative factors have generated constructive maps with a great rate of accuracy. Although the FR method has achieved the highest performance accuracy, the accuracy of the SI and IOE models is considered constructive in assessing the landslides susceptibility in the study area.

### Importance of implemented models and key parameter
In the present investigation, the Seed Cell Area Index (SCAI) method was used to assess the significance of each applied model. SCAI enables proportional calibration between the test dataset with derived landslide susceptibility zones by each applied model (Süzen and Doyuran 2004; Li et al. 2021a, b; Rehman et al. 2022). In the context of SCAI values, higher values in very low susceptibility and lower values in very high susceptibility indicate higher reliability of the model (Rahman et al.

2022). Although the FR model achieved the best reliability according to the SCAI results (Table 5), the other two models also showed a good capability in determining landslide susceptibility in the study area.

Additionally, the relative importance of each key parameter in generating landslide events was calculated depending on the weights calculated in Tables 3 and 4. Figure 9a shows that the slope, lithology, proximity to roads and elevation parameters were the most influential in the FR model. Similarly, lithology, slope and proximity to roads effectively motivated the acceleration of slope materials instability in SI model (Fig. 9b). in IoE model, Fig. 9c depicts the important influence of proximity to faults, proximity to roads and proximity to rivers factors in the creation of landslide events.

### Discussion
Spatial assessment of landslide susceptibility is a critical basis for creating safe spatial development, especially in areas with insufficient spatial data. Thus, many studies aim to produce landslide susceptibility maps using different modelling methods in a GIS environment (Chowdhuri et al. 2020; Tesfa 2022; Zhang et al. 2022). Population and infrastructure are exposed to frequent landslide events in CMA as a result of the complex spatial interaction between a set of physical and human geographical factors. Hitherto, there is a large gap in the national literature concerned with conducting landslide prediction studies. Hence, there is an urgent need to provide

**Table 4** Important factors for landslide susceptibility assessment in the study area with lower IoE value

|  | Parameter | Class | % of landslide | % of domain | $P_{rs}$ | $(P_{rs})$ | $E_s$ | $E_{smax}$ | $I_s$ | $W_f$ |
|---|---|---|---|---|---|---|---|---|---|---|
| 1 | Slope (Degree) | 0–5 | 3.59 | 5.86 | 0.61 | 0.11 | 0.34 | 2.58 | 0.02 | 0.02 |
|  |  | 5–10 | 12.28 | 16.10 | 0.76 | 0.13 | 0.38 |  |  |  |
|  |  | 10–15 | 21.26 | 21.93 | 0.97 | 0.17 | 0.43 |  |  |  |
|  |  | 15–20 | 21.26 | 23.62 | 0.90 | 0.16 | 0.42 |  |  |  |
|  |  | 20–25 | 21.26 | 16.28 | 1.31 | 0.22 | 0.48 |  |  |  |
|  |  | 25< | 20.36 | 16.22 | 1.26 | 0.22 | 0.48 |  |  |  |
| 2 | Slope aspect | Flat | 0.00 | 0.18 | 0.00 | 0.00 | 0.00 | 3.32 | 0.08 | 0.07 |
|  |  | North | 2.69 | 7.10 | 0.38 | 0.05 | 0.20 |  |  |  |
|  |  | Northeast | 3.89 | 7.57 | 0.51 | 0.06 | 0.25 |  |  |  |
|  |  | East | 6.59 | 6.06 | 1.09 | 0.13 | 0.38 |  |  |  |
|  |  | Southeast | 22.46 | 13.39 | 1.68 | 0.20 | 0.47 |  |  |  |
|  |  | South | 25.15 | 18.34 | 1.37 | 0.17 | 0.43 |  |  |  |
|  |  | Southwest | 12.28 | 13.21 | 0.93 | 0.11 | 0.35 |  |  |  |
|  |  | West | 10.48 | 12.40 | 0.84 | 0.10 | 0.34 |  |  |  |
|  |  | Northwest | 11.38 | 14.79 | 0.77 | 0.09 | 0.32 |  |  |  |
|  |  | North | 5.09 | 6.97 | 0.73 | 0.09 | 0.31 |  |  |  |
| 3 | Curvature | Concave | 33.53 | 37.69 | 0.89 | 0.30 | 0.52 | 1.58 | 0.004 | 0.004 |
|  |  | Flat | 23.65 | 24.10 | 0.98 | 0.33 | 0.53 |  |  |  |
|  |  | Convex | 42.81 | 38.22 | 1.12 | 0.37 | 0.53 |  |  |  |
| 4 | Plan curvature | Concave | 26.65 | 31.58 | 0.84 | 0.28 | 0.51 | 1.58 | 0.01 | 0.01 |
|  |  | Flat | 33.23 | 35.51 | 0.94 | 0.31 | 0.52 |  |  |  |
|  |  | Convex | 40.12 | 32.92 | 1.22 | 0.41 | 0.53 |  |  |  |
| 5 | Profile curvature | Concave | 36.53 | 33.30 | 1.10 | 0.37 | 0.53 | 1.58 | 0.01 | 0.04 |
|  |  | Flat | 35.33 | 33.64 | 1.05 | 0.35 | 0.53 |  |  |  |
|  |  | Convex | 28.14 | 33.06 | 0.85 | 0.28 | 0.52 |  |  |  |
| 6 | Elevation | <200 | 0.90 | 1.17 | 0.77 | 0.18 | 0.44 | 2.32 | 0.04 | 0.04 |
|  |  | 200–400 | 4.79 | 11.49 | 0.42 | 0.10 | 0.33 |  |  |  |
|  |  | 400–600 | 16.47 | 23.87 | 0.69 | 0.16 | 0.42 |  |  |  |
|  |  | 600–800 | 31.74 | 26.00 | 1.22 | 0.28 | 0.52 |  |  |  |
|  |  | >800 | 46.11 | 37.47 | 1.23 | 0.28 | 0.52 |  |  |  |
| 7 | NDVI | <0.1 | 0.30 | 0.59 | 0.51 | 0.16 | 0.43 | 2.00 | 0.08 | 0.06 |
|  |  | 0.1–0.3 | 6.29 | 17.86 | 0.35 | 0.11 | 0.36 |  |  |  |
|  |  | 0.3–0.6 | 60.18 | 50.37 | 1.19 | 0.38 | 0.53 |  |  |  |
|  |  | >0.6 | 33.23 | 31.17 | 1.07 | 0.34 | 0.53 |  |  |  |
| 8 | Proximity to faults | <100 | 13.17 | 13.68 | 0.96 | 0.20 | 0.46 | 2.31 | 1.31 | 1.26 |
|  |  | 100–200 | 14.07 | 13.12 | 1.07 | 0.22 | 0.48 |  |  |  |
|  |  | 200–300 | 11.68 | 12.09 | 0.97 | 0.20 | 0.46 |  |  |  |
|  |  | 300–400 | 8.38 | 10.89 | 0.77 | 0.16 | 0.42 |  |  |  |
|  |  | >400 | 52.69 | 50.22 | 1.05 | 0.22 | 0.48 |  |  |  |
| 9 | Proximity to rivers | <100 | 38.92 | 35.05 | 1.11 | 0.27 | 0.51 | 2.20 | 1.20 | 0.99 |
|  |  | 100–200 | 38.02 | 28.69 | 1.33 | 0.32 | 0.53 |  |  |  |
|  |  | 200–300 | 15.57 | 21.70 | 0.72 | 0.17 | 0.44 |  |  |  |
|  |  | 300–400 | 5.99 | 11.41 | 0.52 | 0.13 | 0.38 |  |  |  |
|  |  | >400 | 1.50 | 3.15 | 0.47 | 0.11 | 0.36 |  |  |  |
| 10 | Proximity to roads | <100 | 12.57 | 28.27 | 0.44 | 0.09 | 0.31 | 2.17 | 1.17 | 1.19 |
|  |  | 100–200 | 14.67 | 20.09 | 0.73 | 0.14 | 0.40 |  |  |  |
|  |  | 200–300 | 11.68 | 14.08 | 0.83 | 0.16 | 0.43 |  |  |  |
|  |  | 300–400 | 13.47 | 9.43 | 1.43 | 0.28 | 0.51 |  |  |  |
|  |  | >400 | 47.60 | 28.13 | 1.69 | 0.33 | 0.53 |  |  |  |

**Table 4** (continued)

|    | Parameter | Class | % of landslide | % of domain | $P_{rs}$ | $(P_{rs})$ | $E_s$ | $E_{smax}$ | $I_s$ | $W_f$ |
|----|-----------|-------|----------------|-------------|----------|------------|-------|------------|-------|-------|
| 11 | Rainfall  | <1000 | 1.80 | 4.30 | 0.42 | 0.11 | 0.35 | 2.2 | 1.20 | 0.91 |
|    |           | 1000–1100 | 6.89 | 10.51 | 0.66 | 0.17 | 0.44 | | | |
|    |           | 1100–1200 | 12.28 | 18.34 | 0.67 | 0.18 | 0.44 | | | |
|    |           | 1200–1300 | 13.17 | 19.00 | 0.69 | 0.18 | 0.45 | | | |
|    |           | >1300 | 65.87 | 47.84 | 1.38 | 0.36 | 0.53 | | | |
| 12 | Lithology | C2-3 | 1.80 | 4.32 | 0.42 | 0.06 | 0.25 | 2.62 | 1.62 | 1.22 |
|    |           | J3 | 7.19 | 8.54 | 0.84 | 0.12 | 0.37 | | | |
|    |           | C3 | 25.45 | 29.67 | 0.86 | 0.13 | 0.38 | | | |
|    |           | Bc3 | 1.80 | 7.41 | 0.24 | 0.04 | 0.17 | | | |
|    |           | BN2-b | 0.30 | 2.87 | 0.10 | 0.02 | 0.09 | | | |
|    |           | C4s | 14.07 | 19.30 | 0.73 | 0.11 | 0.34 | | | |
|    |           | C4b | 0.00 | 0.58 | 0.00 | 0.00 | 0.00 | | | |
|    |           | J2 | 43.71 | 24.19 | 1.81 | 0.27 | 0.51 | | | |
|    |           | J1-2 | 5.69 | 3.13 | 1.82 | 0.27 | 0.51 | | | |
| 13 | TWI       | <3 | 87.43 | 83.11 | 1.05 | 0.32 | 0.53 | 1.91 | 0.90 | 0.74 |
|    |           | 3–6 | 10.48 | 13.65 | 0.77 | 0.23 | 0.49 | | | |
|    |           | 6–9 | 0.90 | 2.13 | 0.42 | 0.13 | 0.38 | | | |
|    |           | >9 | 1.20 | 1.12 | 1.07 | 0.32 | 0.53 | | | |
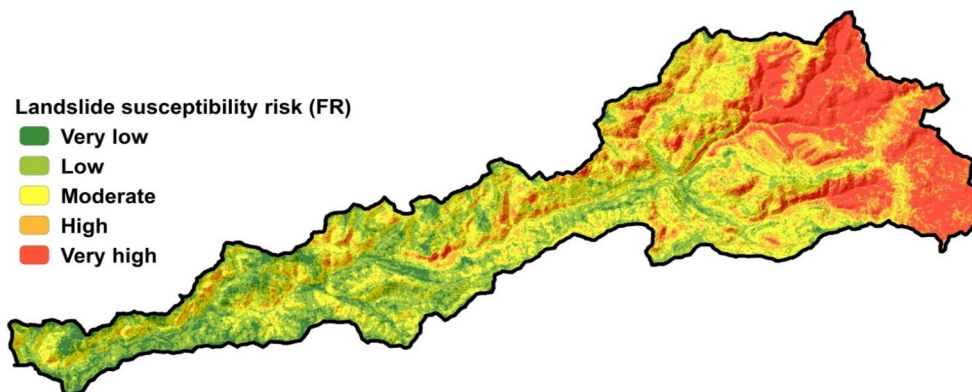


**Fig. 4** Landslide susceptibility map in FRB obtained from the FR model

in-depth spatial assessments of landslide risk that assist in the management and mitigation process. In this evaluation, the performance of three bivariate statistical methods was tested and compared in landslide susceptibility mapping in Al-Balouta river basin.

The inventorization process of landslide events is the primary step in landslide susceptibility modelling. This process involves multiple procedures in areas without documented records of current landslide events. Despite the high frequency of landslide events in most of the watersheds in CMA, there is a loss of historical records for the landslide locations. In the current study, a technical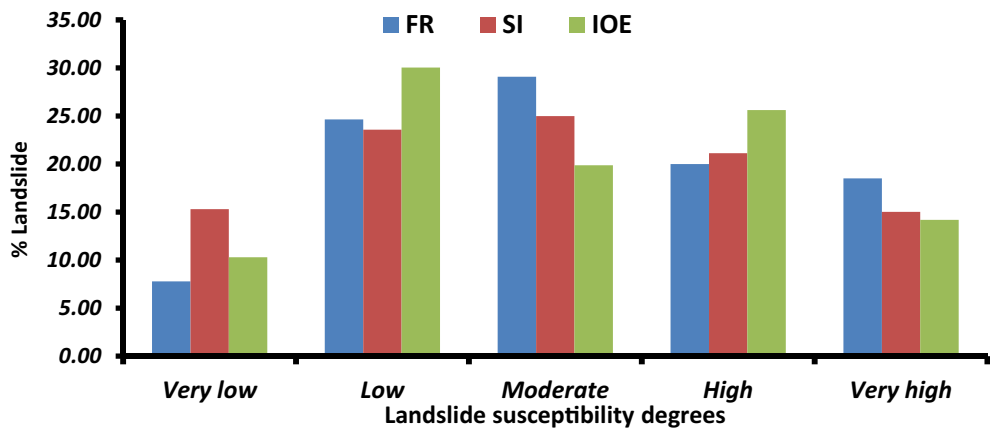-field strategy was based on producing an inventory map of 446 landslide locations. However, this strategy can be relied on in most areas of CMA in generating similar inventory maps for the different types of slope material movement (Es-Smairi et al. 2022). This inventory map enabled a perfect modelling process with thirteen driving factors. The selection of causative factors is a critical task in the context of the most reasonable extraction of landslides using bivariate statistical models (Wubalem et al. 2022). The fieldwork carried out showed the diversity of landslide patterns, including rainfall-induced rapid mass movements, rock falling, bouncing and rolling, shallow landslides and debris and mud flow. These patterns represent a direct reflection of the complex interaction

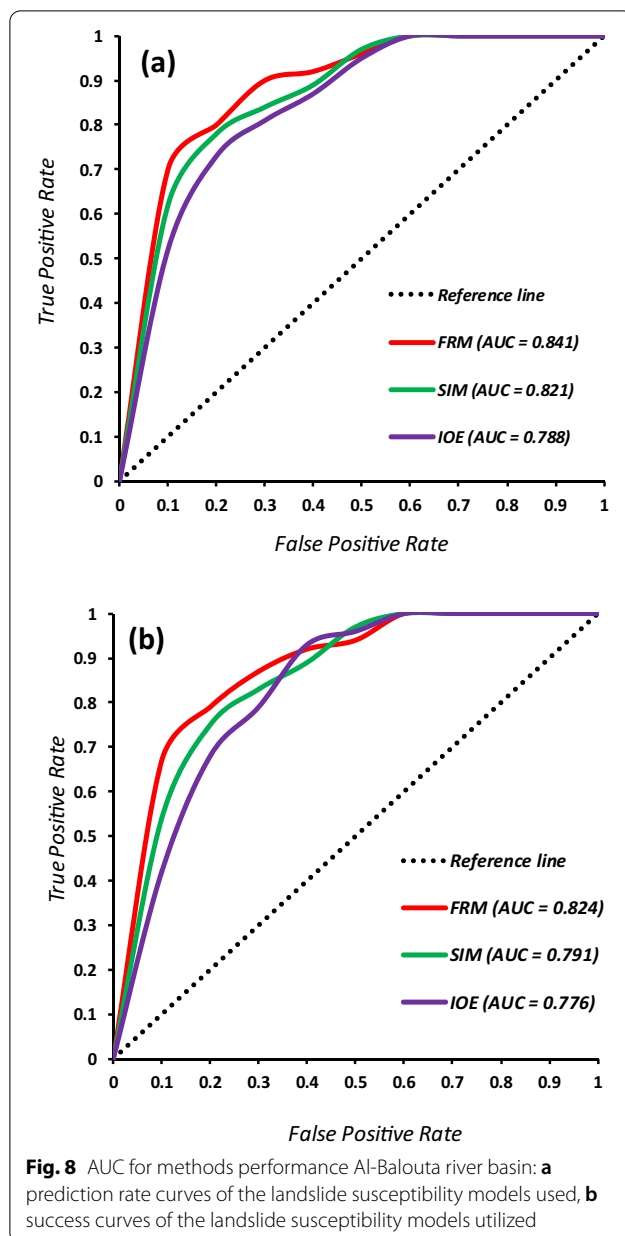Abdo *et al. Geoscience Letters*    (2022) 9:45

Page 18 of 24
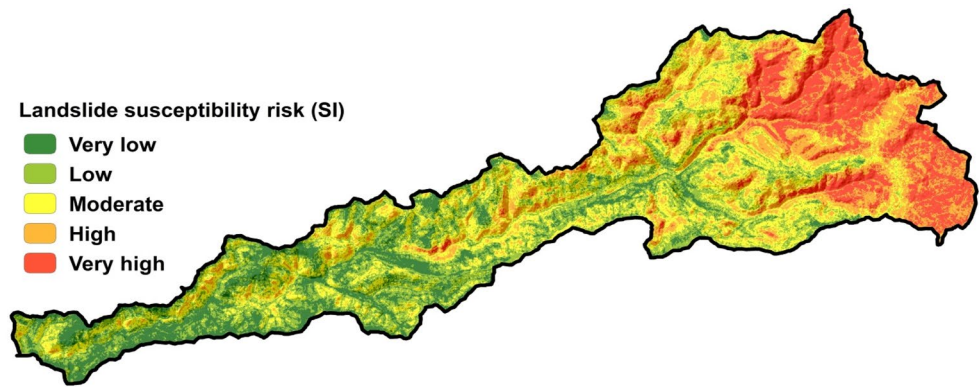


**Fig. 5** Landslide susceptibility map in FRB obtained from the SI model
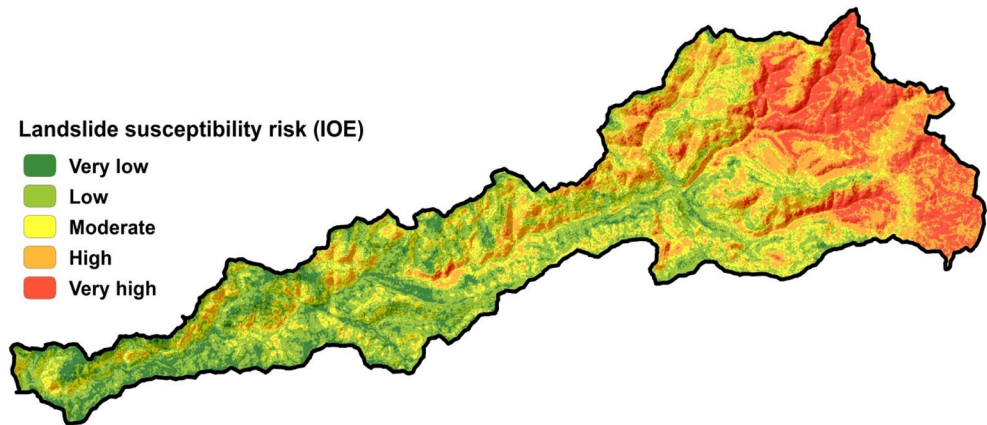


**Fig. 6** Landslide susceptibility map obtained from the IOE model



**Fig. 7** The proportion (%) of landslide pixels for each susceptibility degrees
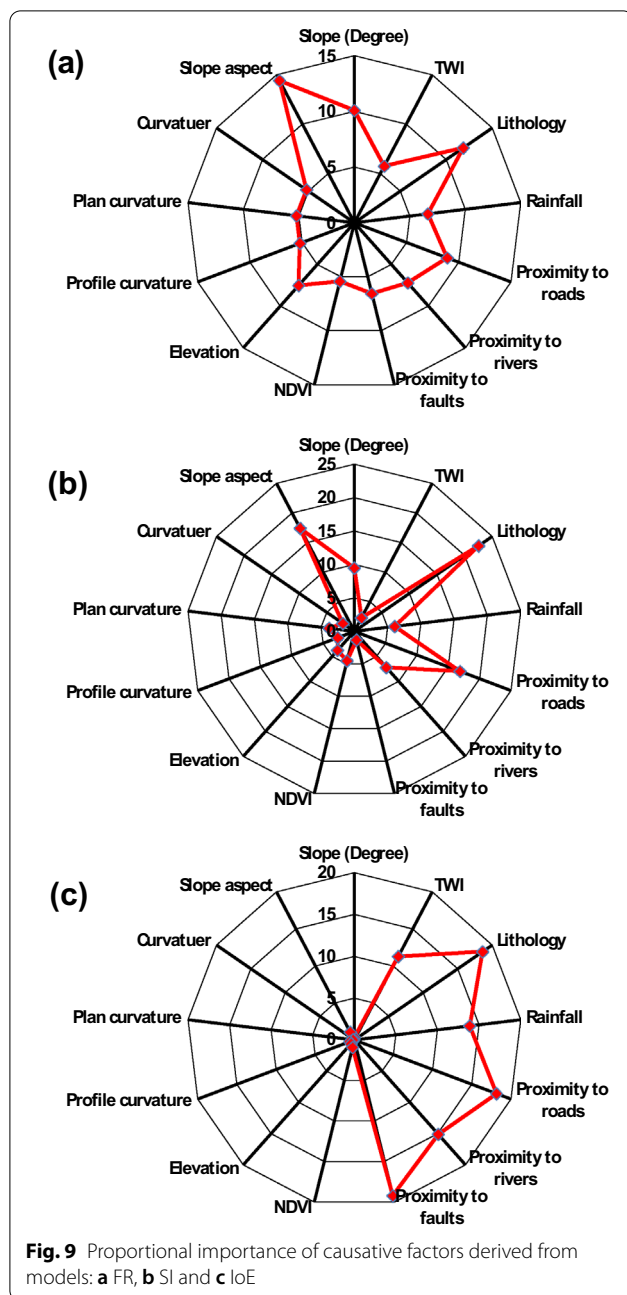
Abdo *et al. Geoscience Letters*      (2022) 9:45

Page 19 of 24



**Fig. 8** AUC for methods performance Al-Balouta river basin: **a** prediction rate curves of the landslide susceptibility models used, **b** success curves of the landslide susceptibility models utilized

between natural and human characteristics in the study area,

Bivariate statistical methods are flexible in implementation with constructive spatial outcomes that assist in managing the landslide risk (Liu et al. 2022; Kincal and Kayhan 2022). In this investigation, the FR model provided the best performance in comparison with the SI and IoE models. In addition to the performance accuracy, the FR model was also identified as the best model in terms of landslide classification capacity. The FR model, however, is based on a direct spatial correlation through the application of an independently relativistic mathematical structure between current landslide events and classifications of causative factors. Thus, direct monitoring of the spatial sensitivity of these classifications through quantitative discrimination of landslide events generation. However, this result allows reducing limitations in this assessment and consistents with landslide assessment studies conducted worldwide (Babitha et al. 2022; Alsabhan et al. 2022; Akter and Javed 2022). Despite the better performance of the FR model, the SI and IoE models also provided reliable performance in landslide susceptibility mapping. In the context of each key factor influencing, slope, lithology and proximity to roads factors were the most influential in landslide events creation. This result is consistent with observations of fieldwork that emphasized the influence of lithological structure and human activity as actual driving factors. Similar results were reported by Tesfa (2022), Senouci et al. (2021) and Yamusa et al. (2022).

In this regard, the outputs of the modelling process indicated that the high and very high landslide susceptibility zones were mainly concentrated in the eastern and northeastern parts with some middle parts along the riverbeds. The fieldwork revealed that the terrain of these areas is characterized by structural fragility and steep slopes with more than 50° in some locations. Also, these areas are characterized by high-intensity rainstorms that cause more landslide events as a result of crossing rainfall thresholds for landslide (Mohammed et al. 2021). These

**Table 5** SCAI value for each landslide susceptibility zone

| Susceptibility zone | FR | | | SI | | | IoE | | |
|---|---|---|---|---|---|---|---|---|---|
| | Area (%) | Landslide events (%) | SCAI | Area | Landslide events (%) | SCAI | Area | Landslide events (%) | SCAI |
| Very low | 7.78 | 4.48 | 1.74 | 15.27 | 13.43 | 1.14 | 10.82 | 6.72 | 1.61 |
| Low | 24.64 | 17.91 | 1.38 | 23.58 | 17.16 | 1.37 | 30.05 | 22.39 | 1.34 |
| Moderate | 29.06 | 17.91 | 1.62 | 25.01 | 17.16 | 1.46 | 19.94 | 20.15 | 0.99 |
| High | 19.99 | 22.39 | 0.89 | 21.13 | 23.13 | 0.91 | 25.01 | 25.37 | 0.99 |
| Very high | 18.52 | 37.31 | 0.50 | 15.01 | 29.10 | 0.52 | 14.18 | 25.37 | 0.56 |

Abdo *et al. Geoscience Letters* (2022) 9:45

Page 20 of 24



**Fig. 9** Proportional importance of causative factors derived from models: **a** FR, **b** SI and **c** IoE

human activity, especially infrastructure projects, has contributed to the instability of slopes. Unfortunately, the spatial distribution of landslide events is not considered when planning these projects. For instance, the road network is built on steep slopes with large loads on slope aspects. These spatial interpretations are consistent with Jamir et al. (2022), Das et al. (2022) and Yamusa et al. (2022).

In this evaluation, FR, SI and IoE models provided a satisfactory performance for a comprehensive assessment of landslides susceptibility in Al-Balouta river basin. The outputs of this study are critical for planners and decision-makers in light of the paucity of relevant geographical data. Moreover, this study represents a constructive contribution in the context of enhancing the national landslides studies, especially during the current war conditions in Syria.

## Conclusion

In this research, landslide hazard maps were produced based on three models (FR, SI and IOE). Although there are advantages and limitations to applying the landslide susceptibility models, they provided a reliable and constructive approach to landslide sensitivity mapping and proved that there is no statistical model that suits all geo-environmental variables. Three alternative statistical approaches were investigated in order to increase the accuracy and flexibility of landslide susceptibility mapping within a GIS framework. To demonstrate the efficiency of the suggested models, a case study of landslide susceptibility mapping in the Al-Balouta river basin in northern Syria is done. The output of this research can be summarized as follows:

1. For FR and SI models, the relevant classes for the selected criteria that have a direct impact on landslide susceptibility were: (1) slopes with 20°–25° and >25°; (2) the slope aspect facing east, southeast and south; (3) convex curvature; (4) elevations between 600 and 800 m and >800 m and >800 m; (5) NDVI ranges between 0.3 and 0.6; (6) proximity to faults between 100 and 200 m; (7) proximity to rivers between 100 and 200 m and <100 m; (8) rainfall >1300 mm, (9) lithology J2 and J1-2; and (10) a greater value of TWI (>9).
2. For IOE model, the most important criteria were: (1) proximity to faults; (2) lithology; (3) proximity to roads; (4) proximity to river; (5) rainfall; and (6) TWI.
3. Based on the three applied models, the landslide hazard maps indicate that 14–18% of the study area was categorized as very high susceptibility to landslide, while 20–25% of the study area was classified into high susceptibility to landslide.

characteristics are integrated with the great acceleration of the karstification process, which causes many slope instability patterns, including karst rockfalls and slides of rocks and soil mixture. Karst land systems are characterized by their significant susceptibility to a combination of physical processes and human activities (Chen et al. 2022). Many studies have indicated a great correlation between the karstification process and landslides, especially in the Mediterranean environment (Devoto et al. 2021; Pisano et al. 2022). Moreover, the acceleration of

Abdo *et al. Geoscience Letters*     (2022) 9:45

Page 21 of 24

4. FR method has achieved the highest performance accuracy, however, the accuracy of the SI and IOE models is considered constructive in assessing the landslides susceptibility in the study area.

5. The relative importance analysis demonstrated that the slope aspects, lithology and proximity to roads effectively motivated the acceleration of slope material instability and were the most influential in both the FR and SI models. On the other hand, the IoE model indicated that the proximity to faults and roads, along with the lithology factor, were important influences in the formation of landslide events.

## Abbreviations
CMA: Coastal mountain area; BSM: Bivariate statistical methods; SRTM: Shuttle Radar Topographic Mission; USGC: United States Geological Survey; LSI: Landslide susceptibility index; DEM: Digital elevation model; FR: Frequency ratio; SI: Statistical index; IoE: Index of entropy; NDVI: Normalized Difference Vegetation Index; TWI: Topographic Wetness Index; AUC: Area under curve; ROC: Receiver-operating characteristics; SCAI: Seed Cell Area Index.

## Supplementary InformationBelow is the link to the electoric supplementary material.

Supplementary file 1 (DOCX 1445 KB)

## Author contributions
H.G.A., H.A., S.A.A. and F.P.: Methodology, H.G.A., H.A. and F.P.: Software, H.A., S.A.A., F.P. and H.A.: Formal analysis and investigation. S.A.A., F.P., S.M. and H.G.A.: visualization, H.G.A., S.A.A., F.P., M.A.M., A.A.A., R.C. and R.C.: Writing—original draft preparation, H.G.A., S.A.A., A.E., K.A., A.A.A. and S.M.: Writing—review and editing, H.A., A.E., R.C., S.M., H.G.A., M.A.M., H.A., K.A. and A.A.A.: Supervision. All authors read and approved the final manuscript.

## Availability of data and materials
The data that support the findings of this study are available on request from the corresponding author.

## Declarations

### Ethics approval and consent to participate
This article does not contain any studies with human participants or animals performed by any of the authors.

### Informed consent
Not applicable.

### Competing interests
The authors have no conflicts of interest to declare.

## Author details
[1]Geography Department, Faculty of Arts and Humanities, University of Tartous, Tartous, Syria. [2]Geography Department, Faculty of Arts and Humanities, Damascus University, Damascus, Syria. [3]Geography Department, Faculty of Arts and Humanities, Tishreen University, Lattakia, Syria. [4]Department of Geography, College of Arabic Language and Social Studies, Qassim University, Burayda 51452, Saudi Arabia. [5]Department of Geography, Faculty of Science, Aligarh Muslim University, Aligarh, UP 202002, India. [6]Agricultural Engineering Department, Faculty of Agriculture, Mansoura University, Mansoura 35516, Egypt. [7]National Institute of Hydrology and Water Management, Bucureşti-Ploieşti Road, 97E, 1st District, 013686 Bucharest, Romania. [8]Danube Delta National Institute for Research and Development, 165 Babadag Street, 820112 Tulcea, Romania. [9]Institute of Land Use, Technical and Precision Technology, Faculty of Agricultural and Food Sciences and Environmental Management, University of Debrecen, Böszörményi 138, Debrecen 4032, Hungary. [10]Department of Geography, College of Arts, Princess Nourah Bint Abdulrahman University, Riyadh 11671, Saudi Arabia. [11]School of Geographical Sciences, Nanjing University of Information Science and Technology, Nanjing 210044, China. [12]Department of Civil Engineering, Transilvania University of Brasov, 5, Turnului Str,, Brasov 500152, Romania. [13]Institutes for Agricultural Research and Educational Farm, University of Debrecen, Böszörményi 138, 4032 Debrecen, Hungary.

## References
Abdo HG (2018) Impacts of war in Syria on vegetation dynamics and erosion risks in Safita area, Tartous, Syria. Reg Environ Chang 18(6):1707–1719. https://doi.org/10.1007/s10113-018-1280-3

Abdo HG (2020) Evolving a total-evaluation map of flash flood hazard for hydro-prioritization based on geohydromorphometric parameters and GIS–RS manner in Al-Hussain river basin, Tartous, Syria. Nat Hazards 104(1):681–703. https://doi.org/10.1007/s11069-020-04186-3

Abdo HG (2021) Assessment of landslide susceptibility zonation using frequency ratio and statistical index: a case study of Al-Fawar basin, Tartous, Syria. Int J Environ Sci Technol 19(4):2599–2618

Abdo HG, Almohamad H, Al Dughairi AA, Al-Mutiry M (2022) GIS-based frequency ratio and analytic hierarchy process for forest fire susceptibility mapping in the western region of Syria. Sustainability 14(8):4668

Abedini M, Ghasemian B, Shirzadi A, Bui DT (2019) A comparative study of support vector machine and logistic model tree classifiers for shallow landslide susceptibility modeling. Environ Earth Sci. https://doi.org/10.1007/s12665-019-8562-z

Abu El-Magd SA, Ali SA, Pham QB (2021) Spatial modeling and susceptibility zonation of landslides using random forest, naïve bayes and K-nearest neighbor in a complicated terrain. Earth Sci Informatics 14(3):1227–1243. https://doi.org/10.1007/s12145-021-00653-y

Akinci H, Yavuz Ozalp A (2021) Landslide susceptibility mapping and hazard assessment in Artvin (Turkey) using frequency ratio and modified information value model. Acta Geophys 69(3):725–745

Akter S, Javed SA (2022) GIS-based assessment of landslide susceptibility and inventory mapping using different bivariate models. Geocarto Int, (just-accepted), 1–31

Ali SA, Parvin F, Vojteková J, Costache R, Linh NTT, Pham QB, Vojtek M, Gigović L, Ahmad A, Ghorbani MA (2021) GIS-based landslide susceptibility modeling: a comparison between fuzzy multi-criteria and machine learning algorithms. Geosci Front 12(2):857–876. https://doi.org/10.1016/j.gsf.2020.09.004

Ali SA, Parvin F, Pham QB, Vojtek M, Vojteková J, Costache R, Linh NTT, Nguyen HQ, Ahmad A, Ghorbani MA (2020) GIS-based comparative assessment of flood susceptibility mapping using hybrid multi-criteria decision-making approach, naïve Bayes tree, bivariate statistics and logistic regression: a case of Topľa basin, Slovakia. Ecol Indic 117(December 2019):106620. https://doi.org/10.1016/j.ecolind.2020.106620

Alsabhan AH, Singh K, Sharma A, Alam S, Pandey DD, Rahman SAS et al (2022) Landslide susceptibility assessment in the Himalayan range based along Kasauli-Parwanoo road corridor using weight of evidence, information value, and frequency ratio. J King Saud Univ-Sci 34(2):101759

Abdo *et al. Geoscience Letters*     (2022) 9:45

Page 22 of 24

Anis Z, Wissem G, Vali V, Smida H, Mohamed Essghaier G (2019) GIS-based landslide susceptibility mapping using bivariate statistical methods in North-western Tunisia. Open Geosci 11(1):708–726. https://doi.org/10.1515/geo-2019-0056

Argyriou AV, Polykretis C, Teeuw RM, Papadopoulos N (2022) Geoinformatic analysis of rainfall-triggered landslides in Crete (Greece) based on spatial detection and hazard mapping. Sustainability 14(7):3956

Babitha BG, Danumah JH, Pradeep GS, Costache R, Patel N, Prasad MK et al (2022) A framework employing the AHP and FR methods to assess the landslide susceptibility of the Western Ghats region in Kollam district. Saf Extreme Environ 4(2):171–191

Batar AK, Watanabe T (2021) Landslide susceptibility mapping and assessment using geospatial platforms and weights of evidence (WoE) method in the Indian himalayan region: Recent developments, gaps, and future directions. ISPRS Int J Geo-Inform. https://doi.org/10.3390/ijgi10030114

Beck HE, Zimmermann NE, McVicar TR, Vergopolan N, Berg A, Wood EF (2018) Present and future Köppen–Geiger climate classification maps at 1-km resolution. Sci Data 5:1–12. https://doi.org/10.1038/sdata.2018.214

Bounemeur N, Benzaid R, Kherrouba H, Atoub S (2022) Landslides in Mila town (northeast Algeria): causes and consequences. Arab J Geosci 15(8):1–15

Bourenane H, Meziani AA, Benamar DA (2021) Application of GIS-based statistical modeling for landslide susceptibility mapping in the city of Azazga, Northern Algeria. Bull Eng Geol Environ 80(10):7333–7359

Bui DT, Moayedi H, Kalantar B, Osouli A, Pradhan B, Nguyen H, Rashid ASA (2019) A novel swarm intelligence—harris hawks optimization for spatial assessment of landslide susceptibility. Sensors (Switzerland). https://doi.org/10.3390/s19163590

Cao Y, Wei X, Fan W, Nan Y, Xiong W, Zhang S (2021) Landslide susceptibility assessment using the weight of evidence method: a case study in Xunyang area, China. PLoS One 16():1–18. https://doi.org/10.1371/journal.pone.0245668

Castro-Miguel R, Legorreta-Paulín G, Bonifaz-Alfonzo R, Aceves-Quesada JF, Castillo-Santiago MÁ (2022) Modeling spatial landslide susceptibility in volcanic terrains through continuous neighborhood spatial analysis and multiple logistic regression in La Ciénega watershed, Nevado de Toluca, Mexico. Nat Hazards 1–22

Chaaban F, El Khattabi J, Darwishe H (2022) Accuracy assessment of ESA WorldCover 2020 and ESRI 2020 land cover maps for a region in Syria. J Geovis Spat Anal 6:31. https://doi.org/10.1007/s41651-022-00126-w

Chen W, Pourghasemi HR, Panahi M, Kornejady A, Wang J, Xie X, Cao S (2017a) Spatial prediction of landslide susceptibility using an adaptive neuro-fuzzy inference system combined with frequency ratio, generalized additive model, and support vector machine techniques. Geomorphology 297:69–85. https://doi.org/10.1016/j.geomorph.2017.09.007

Chen W, Xie X, Wang J, Pradhan B, Hong H, Bui DT, Duan Z, Ma J (2017b) A comparative study of logistic model tree, random forest, and classification and regression tree models for spatial prediction of landslide susceptibility. CATENA 151:147–160. https://doi.org/10.1016/j.catena.2016.11.032

Chen W, Zhang S, Li R, Shahabi H (2018) Performance evaluation of the GIS-based data mining techniques of best-first decision tree, random forest, and naïve Bayes tree for landslide susceptibility modeling. Sci Total Environ 644:1006–1018. https://doi.org/10.1016/j.scitotenv.2018.06.389

Chen F, Bai X, Liu F, Luo G, Tian Y, Qin L et al (2022) Analysis long-term and spatial changes of forest cover in typical karst areas of China. Land 11(8):1349

Chiranjit, Singha Kishore Chandra, Swain Modeste, Meliho Hazem Ghassan, Abdo Hussein, Almohamad Motirh, Al-Mutiry (2022) Spatial Analysis of Flood Hazard Zoning Map Using Novel Hybrid Machine Learning Technique in Assam India. Remote Sensing 14(24) 6229-10.3390/rs14246229

Chowdhuri I, Pal SC, Arabameri A, Ngo PTT, Chakrabortty R, Malik S et al (2020) Ensemble approach to develop landslide susceptibility map in landslide dominated Sikkim Himalayan region, India. Environ Earth Sci 79(20):1–28

Costache R (2019) Flash-Flood Potential assessment in the upper and middle sector of Prahova river catchment (Romania). A comparative approach between four hybrid models. Sci Total Environ 659:1115–1134. https://doi.org/10.1016/j.scitotenv.2018.12.397

Costache R, Tien Bui D (2020) Identification of areas prone to flash-flood phenomena using multiple-criteria decision-making, bivariate statistics, machine learning and their ensembles. Sci Total Environ 712:136492. https://doi.org/10.1016/j.scitotenv.2019.136492

Das S, Sarkar S, Kanungo DP (2022) GIS-based landslide susceptibility zonation mapping using the analytic hierarchy process (AHP) method in parts of Kalimpong Region of Darjeeling Himalaya. Environ Monit Assess 194(3):1–28

Devoto S, Hastewell LJ, Prampolini M, Furlani S (2021) Dataset of gravity-induced landforms and sinkholes of the northeast Coast of Malta (Central Mediterranean Sea). Data 6(8):81

Di B, Zhang H, Liu Y, Li J, Chen N, Stamatopoulos CA, Luo Y, Zhan Y (2019) Assessing susceptibility of debris flow in southwest China using gradient boosting machine. Sci Rep 9(1):1–12. https://doi.org/10.1038/s41598-019-48986-5

Dikshit A, Sarkar R, Pradhan B, Segoni S, Alamri AM (2020) Rainfall induced landslide studies in Indian Himalayan region: a critical review. Appl Sci 10(7):1–24. https://doi.org/10.3390/app10072466

Eitvandi N, Sarikhani R, Derikvand S (2022) Landslide susceptibility mapping by integrating analytical hierarchy process, frequency ratio, and fuzzy gamma operator models, case study: North of Lorestan Province, Iran. Environ Monit Assessm 194(9):1–26

Emberson R, Kirschbaum D, Stanley T (2021) Global connections between El Nino and landslide impacts. Nat Commun 12(1):1–11. https://doi.org/10.1038/s41467-021-22398-4

Es-Smairi A, El Moutchou B, El Ouazani Touhami A, Namous M, Mir RA (2022). Landslide susceptibility mapping using GIS-based bivariate models in the Rif chain (northernmost Morocco). Geocarto Int 1–31

Fan X, Scaringi G, Korup O, West AJ, van Westen CJ, Tanyas H, Hovius N, Hales TC, Jibson RW, Allstadt KE, Zhang L, Evans SG, Xu C, Li G, Pei X, Xu Q, Huang R (2019) Earthquake-induced chains of geologic hazards: patterns, mechanisms, and impacts. Rev Geophys 57(2):421–503. https://doi.org/10.1029/2018RG000626

Fang Z, Wang Y, Duan G, Peng L (2021) Landslide susceptibility mapping using rotation forest ensemble technique with different decision trees in the three gorges reservoir area, China. Remote Sens 13(2):1–22. https://doi.org/10.3390/rs13020238

Guo X, Fu B, Du J, Shi P, Li J, Li Z, Du J, Chen Q, Fu H (2021) Monitoring and assessment for the susceptibility of landslide changes after the 2017 Ms 7.0 jiuzhaigou earthquake using the remote sensing technology. Front Earth Sci 9(February):1–17. https://doi.org/10.3389/feart.2021.633117

Hamza T, Raghuvanshi TK (2017) GIS based landslide hazard evaluation and zonation—a case from Jeldu District, Central Ethiopia, GIS based landslide hazard evaluation and zonation. J King Saud Univ Sci 29(2):151–165. https://doi.org/10.1016/j.jksus.2016.05.002

Hateffard F, Mohammed S, Alsafadi K, Enaruvbe GO, Heidari A, Abdo HG, Rodrigo-Comino J (2021) CMIP5 climate projections and RUSLE-based soil erosion assessment in the central part of Iran. Sci Rep 11(1):1–17. https://doi.org/10.1038/s41598-021-86618-z

He Q, Wang M, Liu K (2021) Rapidly assessing earthquake-induced landslide susceptibility on a global scale using random forest. Geomorphology 391:107889

Zhu K, Xu P, Cao C, Zheng L, Liu Y, Dong X (2021) Preliminary identification of geological hazards from Songpinggou to Feihong in Mao county along the Minjiang river using SBAS-InSAR technique integrated multiple spatial analysis methods. Sustainability 13(3):1017

Hepdeniz K (2020) Using the analytic hierarchy process and frequency ratio methods for landslide susceptibility mapping in Isparta-Antalya highway (D-685), Turkey. Arab J Geosci. https://doi.org/10.1007/s12517-020-05764-2

Huang Y, Zhao L (2018) Review on landslide susceptibility mapping using support vector machines. CATENA 165(January):520–529. https://doi.org/10.1016/j.catena.2018.03.003

Jaafari A, Janizadeh S, Abdo HG, Mafi-Gholami D, Adeli B (2022) Understanding land degradation induced by gully erosion from the perspective of different geoenvironmental factors. J Environ Manage 315:115181

Jamir M, Chang CN, Jamir I, Thong GT, Walling T (2022) Landslide susceptibility mapping of Noklak Town, Nagaland, North-east India using bivariate statistical method. Geol J

Abdo *et al. Geoscience Letters*    (2022) 9:45

Page 23 of 24

Jana SK, Sekac T, Pal DK (2019) Geo-spatial approach with frequency ratio method in landslide susceptibility mapping in the Busu River catchment, Papua New Guinea. Spatial Inform Res 27(1):49–62

Karam, Alsafadi Shuoben, Bi Hazem Ghassan, Abdo Mario J., Al Sayah Tamás, Ratonyi Endre, Harsanyi Safwan, Mohammed Spatial–temporal dynamic impact of changes in rainfall erosivity and vegetation coverage on soil erosion in the Eastern Mediterranean. Environmental Science and Pollution Research 10.1007/s11356-022-24012-6

Karaman MO, Çabuk SN, Pekkan E (2022) Utilization of frequency ratio method for the production of landslide susceptibility maps: Karaburun Peninsula case, Turkey. Environ Sci Pollut Res 1–21

Karim Z, Hadji R, Hamed Y (2019) GIS-based approaches for the landslide susceptibility prediction in Setif Region (NE Algeria). Geotech Geol Eng 37(1):359–374

Karlsson CSJ, Kalantari Z, Mörtberg U, Olofsson B, Lyon SW (2017) Natural hazard susceptibility assessment for road planning using spatial multi-criteria analysis. Environ Manage 60(5):823–851. https://doi.org/10.1007/s00267-017-0912-6

Kincal C, Kayhan H (2022) A combined method for preparation of landslide susceptibility map in Izmir (Türkiye). Appl Sci 12(18):9029

Kumar R, Anbalagan R (2016) Landslide susceptibility mapping using analytical hierarchy process (AHP) in Tehri reservoir rim region, Uttarakhand. J Geol Soc India 87(3):271–286. https://doi.org/10.1007/s12594-016-0395-8

Li Y, Mo P (2019) A unified landslide classification system for loess slopes: a critical review. Geomorphology 340:67–83. https://doi.org/10.1016/j.geomorph.2019.04.020

Li B, Wang N, Chen J (2021a) GIS-based landslide susceptibility mapping using information, frequency ratio, and artificial neural network methods in Qinghai Province, Northwestern China. Adv Civ Eng. https://doi.org/10.1155/2021/4758062

Li J, Wang W, Li Y, Han Z, Chen G (2021b) Spatiotemporal landslide susceptibility mapping incorporating the effects of heavy rainfall: a case study of the heavy rainfall in August 2021 in Kitakyushu, Fukuoka, Japan. Water 13(22):3312

Lin Q, Lima P, Steger S, Glade T, Jiang T, Zhang J et al (2021) National-scale data-driven rainfall induced landslide susceptibility mapping for China by accounting for incomplete landslide data. Geosci Front 12(6):101248

Liu Y, Yuan A, Bai Z, Zhu J (2022) GIS-based landslide susceptibility mapping using frequency ratio and index of entropy models for She County of Anhui Province, China. Appl Rheol 32(1):22–33

Ma S, Qiu H, Hu S, Pei Y, Yang W, Yang D, Cao M (2020) Quantitative assessment of landslide susceptibility on the Loess Plateau in China. Phys Geogr 41(6):489–516. https://doi.org/10.1080/02723646.2019.1674559

Mavroulis S, Diakakis M, Kranis H, Vassilakis E, Kapetanidis V, Spingos I et al (2022) Inventory of historical and recent earthquake-triggered landslides and assessment of related susceptibility by GIS-based analytic hierarchy process: the case of Cephalonia (Ionian Islands, Western Greece). Appl Sci 12(6):2895

Mersha T, Meten M (2020) GIS-based landslide susceptibility mapping and assessment using bivariate statistical methods in Simada area, northwestern Ethiopia. Geoenviron Disasters. https://doi.org/10.1186/s40677-020-00155-x

Mind'je R, Li L, Nsengiyumva JB, Mupenzi C, Nyesheja EM, Kayumba PM, Gasirabo A, Hakorimana E, (2020) Landslide susceptibility and influencing factors analysis in Rwanda. Environ Dev Sustain 22(8):7985–8012. https://doi.org/10.1007/s10668-019-00557-4

Mohammed S, Abdo HG, Szabo S, Pham QB, Holb IJ, Linh NTT, Anh DT, Alsafadi K, Mokhtar A, Kbibo I, Ibrahim J, Rodrigo-Comino J (2020a) Estimating human impacts on soil erosion considering different hillslope inclinations and land uses in the coastal region of Syria. Water 12(10):2786. https://doi.org/10.3390/w12102786

Mohammed S, Hassan E, Abdo HG, Szabo S, Mokhtar A, Alsafadi K, Al-Khouri I, Rodrigo-Comino J (2021) Impacts of rainstorms on soil erosion and organic matter for different cover crop systems in the western coast agricultural region of Syria. Soil Use Manage 37(1):196–213. https://doi.org/10.1111/sum.12683

Mohammed S, Al-Ebraheem A, Holb IJ, Alsafadi K, Dikkeh M, Pham QB, Linh NTT, Szabo S (2020b) Soil management effects on soil water erosion and runoff in Central Syria—a comparative evaluation of general linear

model and random forest regression. Water (Switzerland). https://doi.org/10.3390/w12092529

Naceur HA, Abdo HG, Igmoullan B, Namous M, Almohamad H, Al Dughairi AA, Al-Mutiry M (2022) Performance assessment of the landslide susceptibility modelling using the support vector machine, radial basis function network, and weight of evidence models in the N'fis river basin, Morocco. Geosci Lett 9(1):1–20

Nakileza BR, Nedala S (2020) Topographic influence on landslides characteristics and implication for risk management in upper Manafwa catchment, Mt Elgon Uganda. Geoenviron Disasters. https://doi.org/10.1186/s40677-020-00160-0

Pham QB, Achour Y, Ali SA, Parvin F, Vojtek M, Vojteková J, Al-Ansari N, Achu AL, Costache R, Khedher KM, Anh DT (2021a) A comparison among fuzzy multi-criteria decision making, bivariate, multivariate and machine learning models in landslide susceptibility mapping. Geomatics Nat Hazards Risk 12(1):1741–1777. https://doi.org/10.1080/19475705.2021.1944330

Pham BT, Van Dao D, Acharya TD, Van Phong T, Costache R, Van Le H et al (2021b) Performance assessment of artificial neural network using chi-square and backward elimination feature selection methods for landslide susceptibility analysis. Environ Earth Sci 80(20):1–13

Pisano L, Zumpano V, Pepe M, Liso IS, Parise M (2022) Assessing karst landscape degradation: a case study in southern Italy. Land 11(10):1842

Ponikarov VP, Kazmin VG, Mikhailov IA, Razvaliayev AV, Krasheninnikov VA, Kozlov VV et al (1967) The geology of Syria: explanatory notes on the geological map of Syria, scale 1: 500 000, part I: Stratigraphy, igneous rocks, and tectonics. Ministry of Industry, Damascu

Pourghasemi HR, Mohammady M, Pradhan B (2012) Landslide susceptibility mapping using index of entropy and conditional probability models in GIS: Safarood Basin. Iran Catena 97:71–84. https://doi.org/10.1016/j.catena.2012.05.005

Psomiadis E, Papazachariou A, Soulis KX, Alexiou DS, Charalampopoulos I (2020) Landslide mapping and susceptibility assessment using geospatial analysis and earth observation data. Land. https://doi.org/10.3390/LAND9050133

Rahman G, Bacha AS, Ul Moazzam MF, Rahman AU, Mahmood S, Almohamad H, Abdo HG (2022) Assessment of landslide susceptibility, exposure, vulnerability, and risk in shahpur valley, eastern hindu kush. Front Earth Sci 1348

Razavizadeh S, Solaimani K, Massironi M, Kavian A (2017) Mapping landslide susceptibility with frequency ratio, statistical index, and weights of evidence models: a case study in northern Iran. Environ Earth Sci. https://doi.org/10.1007/s12665-017-6839-7

Rehman A, Song J, Haq F, Mahmood S, Ahamad MI, Basharat M et al (2022) Multi-hazard susceptibility assessment using the analytical hierarchy process and frequency ratio techniques in the Northwest Himalayas. Pak Remote Sens 14(3):554

Reichenbach P, Rossi M, Malamud BD, Mihir M, Guzzetti F (2018a) A review of statistically-based landslide susceptibility models. Earth-Science Rev 180(March):60–91. https://doi.org/10.1016/j.earscirev.2018.03.001

Reichenbach P, Rossi M, Malamud BD, Mihir M, Guzzetti F (2018b) A review of statistically-based landslide susceptibility models. Earth Sci Rev 180:60–91

Sachdeva S, Bhatia T, Verma AK (2020) A novel voting ensemble model for spatial prediction of landslides using GIS. Int J Remote Sens 41(3):929–952. https://doi.org/10.1080/01431161.2019.1654141

Sahana M, Pham BT, Shukla M, Costache R, Thu DX, Chakrabortty R, Satyam N, Nguyen HD, Van PT, Van LH, Pal SC, Areendran G, Imdad K, Prakash I (2020) Rainfall induced landslide susceptibility mapping using novel hybrid soft computing methods based on multi-layer perceptron neural network classifier. Geocarto Int. https://doi.org/10.1080/10106049.2020.1837262

Saibal, Ghosh Emmanuel John M., Carranza Cees J., van Westen Victor G., Jetten Dipendra N., Bhattacharya (2011) Selecting and weighting spatial predictors for empirical modeling of landslide susceptibility in the Darjeeling Himalayas (India). Geomorphology 131(1-2) 35-56 S0169555X11001887 10.1016/j.geomorph.2011.04.019

Sajjad, Hussain Shujing, Qin Wajid, Nasim Muhammad Adnan, Bukhari Muhammad, Mubeen Shah, Fahad Ali, Raza Hazem Ghassan, Abdo Aqil, Tariq B. G., Mousa Faisal, Mumtaz Muhammad, Aslam (2022) Monitoring the Dynamic Changes in Vegetation Cover Using Spatio-Temporal Remote

Sensing Data from 1984 to 2020. Atmosphere 13(10) 1609-10.3390/atmos13101609

Saleh, Yousefi Somayeh, Mirzaee Hussein, Almohamad Ahmed Abdullah, Al Dughairi Christopher, Gomez Narges, Siamian Mona, Alrasheedi Hazem Ghassan, Abdo (2022) Image Classification and Land Cover Mapping Using Sentinel-2 Imagery: Optimization of SVM Parameters. Land 11(7) 993-10.3390/land11070993

Senouci R, Taibi NE, Teodoro AC, Duarte L, Mansour H, Yahia Meddah R (2021) GIS-based expert knowledge for landslide susceptibility mapping (LSM): case of mostaganem coast district, west of Algeria. Sustainability 13(2):630

Shafapour Tehrany M, Kumar L, Neamah Jebur M, Shabani F (2019) Evaluating the application of the statistical index method in flood susceptibility mapping and its comparison with frequency ratio and logistic regression methods. Geomatics Nat Hazards Risk 10(1):79–101. https://doi.org/10.1080/19475705.2018.1506509

Shi JJ, Zhang W, Wang B, Li CY, Pan B (2020) Simulation of a submarine landslide using the coupled material point method. Math Probl Eng. https://doi.org/10.1155/2020/4392581

Skrzypczak I, Kokoszka W, Zientek D, Tang Y, Kogut J (2021) Landslide hazard assessment map as an element supporting spatial planning: the flysch carpathians region study. Remote Sens 13(2):1–20. https://doi.org/10.3390/rs13020317

Süzen ML, Doyuran V (2004) A comparison of the GIS based landslide susceptibility assessment methods: multivariate versus bivariate. Environ Geol 45(5):665–679

Tesfa C (2022) GIS-based AHP and FR methods for landslide susceptibility mapping in the Abay Gorge, Dejen-Renaissance Bridge, Central, Ethiopia. Geotechn Geol Eng 40(10):5029–5043

Thapa PB, Esaki T (1970) GIS-based quantitative landslide hazard prediction modelling in natural hillslope, Agra Khola watershed, central Nepal. Bull Dep Geol 10:63–70. https://doi.org/10.3126/bdg.v10i0.1421

Ullah I, Aslam B, Shah SHIA, Tariq A, Qin S, Majeed M, Havenith HB (2022) An integrated approach of machine learning, remote sensing, and GIS data for the landslide susceptibility mapping. Land 11(8):1265

Valiante M, Guida D, Della Seta M, Bozzano F (2021) A spatiotemporal object-oriented data model for landslides (LOOM). Landslides 18(4):1231–1244. https://doi.org/10.1007/s10346-020-01591-4

Vincent E, Nwazelibe Chinanu O, Unigwe Johnbosco C, Egbueri Integration and comparison of algorithmic weight of evidence and logistic regression in landslide susceptibility mapping of the Orumba North erosion-prone region Nigeria. Modeling Earth Systems and Environment 10.1007/s40808-022-01549-6

Wu Y, Ke Y, Chen Z, Liang S, Zhao H, Hong H (2020) Application of alternating decision tree with AdaBoost and bagging ensembles for landslide susceptibility mapping. Catena 187(November 2019):104396. https://doi.org/10.1016/j.catena.2019.104396

Wubalem A (2021) Landslide susceptibility mapping using statistical methods in Uatzau catchment area, northwestern Ethiopia. Geoenviron Disasters 8(1):1–21

Wubalem A, Getahun B, Hailemariam Y, Mesele A, Tesfaw G, Dawit Z, Goshe E (2022) Landslide susceptibility modeling using the index of entropy and frequency ratio method from Nefas-Mewcha to Weldiya Road Corridor, Northwestern Ethiopia. Geotechn Geol Eng 40(10):5249–5278

Yamusa IB, Ismail MS, Tella A (2022) Highway proneness appraisal to landslides along Taiping to Ipoh Segment Malaysia, using MCDM and GIS techniques. Sustainability 14(15):9096

Youssef AM, Al-Kathery M, Pradhan B (2015) Landslide susceptibility mapping at Al-Hasher area, Jizan (Saudi Arabia) using GIS-based frequency ratio and index of entropy models. Geosci J 19(1):113–134. https://doi.org/10.1007/s12303-014-0032-8

Yu C, Liu K, Yu B, Yin J (2022) GIS-based study on the susceptibility of shallow landslides: a case study of mass shallow landslides in Sanming, Fujian in 2019. Nat Hazards 1–23.

Zhang T, Han L, Zhang H, Zhao Y, Li X, Zhao L (2019) GIS-based landslide susceptibility mapping using hybrid integration approaches of fractal dimension with index of entropy and support vector machine. J Mater Sci 16(6):1275–1288. https://doi.org/10.1007/s11629-018-5337-z

Zhang T, Quevedo RP, Wang H, Fu Q, Luo D, Wang T et al (2022) Improved tree-based machine learning algorithms combining with bagging strategy for landslide susceptibility modeling. Arab J Geosci 15(2):1–19

Zhou C, Yin K, Cao Y, Ahmed B, Li Y, Catani F, Pourghasemi HR (2018) Landslide susceptibility modeling applying machine learning methods: a case study from Longju in the Three Gorges Reservoir area, China. Comput Geosci 112:23–37

## Publisher's Note